EFFECTS OF COLLISIONS WITH ROCKY PLANETS ON THE STRUCTURE OF HOT JUPITERS

Kassandra R. Anderson

Honors Senior Thesis

Research Advisor: Fred C. Adams

Department of Physics, University of Michigan

ABSTRACT

The observed Hot Jupiters exhibit a wide range of physical properties. For a given mass, many planets have inflated radii, while others are surprisingly compact and may harbor large central cores. Motivated by this observational sample, this thesis considers the possible effects from collisions between Jovian planets and smaller rocky planets, and investigates whether these radius anomalies could be explained (in part) by such collisions. In this scenario, Jovian planets migrate through the circumstellar disk and enter into ~ 4 day orbits, whereas the rocky planets (with mass $m_{\rm p} = 0.1 - 20 M_\oplus$) migrate later and then encounter the Jovian planets. This thesis calculates the trajectories of incoming rocky planets as they orbit within the gaseous planets and are subjected to gravitational, frictional, and tidal forces. Such collisions cause the metallicity of the Jovian planet to increase, and if the rocky planets survive tidal disruption and reach the central regions, provide a means of producing large planetary cores. The energy released during these collisions provides the Jovian planet with an additional energy source and could inflate the radius; here we determine the radial layers where the kinetic energy is dissipated, including the energy remaining upon impact with the existing core. This process could have long-term effects if the colliding body deposits significant amounts of mass and energy deep in the interior, in regions of high opacity.

1. Introduction

Since the first discovery of an exoplanet orbiting a main-sequence star (Mayor & Queloz 1995), the field of extrasolar planets has undergone rapid progress. More than 750 additional planets have been observed, with over 1000 more possible objects awaiting further measurements for confirmation (Borucki et al. 2011). Although the observational sample is far from complete, it is clear that the galaxy hosts a diverse population of planets, with a range of masses spanning over three orders of magnitude. Over 150 of the ~ 750 confirmed planets are gaseous planets similar to Jupiter, but with semi-major axes less than 0.1 AU. Such proximity to their host stars causes these planets to intercept high levels of radiation and reach surface temperatures greater than 1000 K. These planets reach such extreme environments by forming further out in the circumstellar disk and migrating inward (Papaloizou & Terquem 2006). Up to $\sim 5\%$ of all solar systems are believed to harbor "Hot Jupiters" (Bramich & Horne 2006; van Saders & Gaudi 2011), and therefore a billion such planets could reside in the galaxy. Their combination of large masses and short orbital periods has made the Hot Jupiters particularly suitable targets for transit observations, where the planet passes in front of its host star and causes a measurable drop in the stellar intensity. With the advent of both space and ground-based observatories, the number of planets detected via the transit method continues to grow. This technique, coupled with traditional radial velocity observations, allows both the planetary mass and radius to be determined.

The observed Hot Jupiters have a range of radii for a given mass (Baraffe et al. 2010). Many planets are larger than predicted, but some are also surprisingly small. The reasons for these anomalous radii remain unknown, and the construction of a mass-radius theory for the Hot Jupiters has become a central problem in exoplanet research. The inflated planets can be understood if they contain additional internal energy sources (Bodenheimer et al. 2003; Gu et al. 2004), and numerous heating mechanisms and their implications have been discussed (Laughlin et al. 2011), e.g., heat generated by Ohmic dissipation (Batygin & Stevenson 2010; Perna et al 2010; Batygin et al. 2011), conversion of wind kinetic energy into heat (Rauscher & Menou 2012; Guillot & Showman 2002), and/or tidal dissipation (Arras & Socrates 2010). In contrast, the giant planets with deflated radii have high metallicities and possibly large cores (Burrows et al. 2007). The problem of these anomalous radii thus splits into two sub-problems: the source(s) of additional heating, and the ways in which planets can increase their metallicity and accumulate large cores. Identifying possible long-term heat sources and examining the ways in which planets can increase their core masses will help explain the observed radius distribution and further our understanding of giant planet formation, structure, and evolution.

This thesis explores whether these radius anomalies could result from the accretion of

smaller terrestrial planets, soon after the formation and inward migration of the giant planet. During the early epochs of solar system formation, a large number of small terrestrial bodies are present, and previous work has shown that they can migrate inward and become captured by a Hot Jupiter with high probability (Ketchum et al. 2011b) . After capture, a rocky planet orbiting within the atmosphere of a Jovian planet loses energy due to damping forces and eventually either collides with the existing core or becomes tidally disrupted. A substantial amount of energy can be released during the collision. This energy could inflate the giant planet over a long period of time, provided that sufficient energy is deposited deep in the planet interior, where the opacity is high. On the other hand, if most of the energy is dissipated in the outer planetary layers, it would provide only a short-term source of energy. In addition to providing a possible energy source, such impacts are a natural mechanism for increasing a planet's metallicity, and could help explain some of the metal-rich compositions and large cores of the Hot Jupiters. These impacts could thus help explain, in part, both of the observed radius anomalies.

Given the strong observational evidence for planets with large cores, the process of core accumulation is of particular interest. An example is given by the planet HD 149026b, with a total mass $M_P = 0.36 \pm 0.03 M_J$, and radius $R_P = 0.73 \pm 0.03 R_J$ (Sato et al. 2005). These observational constraints, along with theoretical calculations (Fortney et al. 2006; Ikoma et al. 2006), indicate that this planet contains $80 M_\oplus$ of heavy elements. A significant fraction of these heavy elements could reside in the core. Although observations cannot yet constrain the exact mass of the core, it is expected that HD 149026b and other planets have larger cores than predicted by theoretical models of giant planet formation. According to the core accretion model (Pollack et al. 1996), giant planet cores are formed from rocky planetesimals in the circumstellar disk, and after reaching a critical mass around $10 M_\oplus$ begin to accrete gas. Sufficiently large planets experience runaway gas accretion and clear gaps in their disks, so that the accretion of additional rocky material is suppressed. It is thus difficult to build up a core mass as high as $80 M_\oplus$ by means of this process. An alternative model is the formation of giant planets via gravitational instabilities in the circumstellar disk (Boss 1997). Planets formed through this process would have essentially the same composition as their host stars, which is difficult to reconcile with the enhanced metallicities of most extrasolar planets, as well as our own Jupiter and Saturn. These issues motivate the possible role of collisions in giant planet core formation.

The accretion of small objects (planetesimals, with radius $r_{\rm p} \approx 1 - 100$ km) by Jovian planet embryos has been modeled (e.g., Helled et al. 2006; Benvenuto & Brunini 2008); however, the accretion of larger rocky bodies could also be important in giant planet formation. A planet with an initially small core mass could accrete one or more large rocky planets ($m_{\rm p} \gtrsim 1 M_\oplus$) early in its lifetime and thereby accumulate a heavy core. Collisions with

"superearths" ($m_{\rm p} \approx 10 M_\oplus$) are probably the best way to explain the most massive cores, since the accumulation of a large core from low-mass planets would require an unrealistic frequency of encounters. In addition, as we show in this thesis, small planets are unlikely to survive the entire trajectory and reach the central regions of the Jovian planet. However, as previous work has shown (e.g., Benvenuto & Brunini 2008), the accretion of smaller planets can alter the structure of the giant planet in other aspects, such as by increasing the metallicity of envelope.

Here we model the collisional dynamics between a Jovian planet and a rocky planet, and consider the effects of these collisions on the metallicity, core size, and energy budget of the Jovian planet. This problem has been explored by others, in the context of Jupiter and Saturn (Anic et al. 2007; Li et al. 2010) via smooth particle hydrodynamical (SPH) simulations. These authors have investigated both the overall effects on the structure of the giant planet, as well as the survival of the colliding bodies. The conditions for rocky planets to survive are particularly important. Their results indicate that low mass planets $m_{\rm p} \approx 1 M_\oplus$ are often destroyed prior to reaching the core, while superearths usually survive the entire trajectory. This thesis extends this previous work, but uses a different approach. SPH (or equivalent) methods provide a detailed description of the collisions, but are computationally expensive and allow relatively few cases to be considered. Here, instead, we treat the collision as a one-body problem, where the incoming projectile planet orbits within the giant target planet and is subjected to gravitational, frictional, and tidal forces. This approach allows for a much wider survey of the parameter space, which, in spite of the simplifying approximations, increases our physical understanding of these collisions. This thesis investigates the accretion of rocky bodies spanning two orders of magnitude ($m_{\rm p} = 0.1 - 20 M_\oplus$), within a Jovian planet of varying properties. Here we consider Jovian planets with mass $M_P = 1 M_J$ and radius $R_P = 1 - 2 R_J$, where the latter are appropriate for young Jovian planets (Burrows et al. 1997). Note that M_J and R_J denote the mass and radius of Jupiter.

This paper is organized as follows: In Section 2, we develop a structure model of a gaseous giant planet using a polytropic equation of state. Using this model in Section 3, we calculate the orbits of incoming rocky bodies within the giant planet atmosphere, and determine the likelihood that the rocky body is captured. We also examine the energy dissipation as a function of radial distance and calculate the remaining kinetic energy upon impact with the existing core. In Section 4 we calculate the tidal forces exerted by the Jovian planet as a function of radial distance, and determine whether the rocky planets can survive tidal disruption. We conclude, in Section 5 with a summary of our results and a discussion of their implications.

The main body of this thesis is supplemented by three appendices. In Appendix A, we

derive an estimate of the expected frequency of collisions, using simple circumstellar disk models. In Appendix B, we discuss the dynamics of a test particle orbiting in a polytropic potential, in the limit of small distance from the origin. Finally, in Appendix C, we apply the methods of Section 4 to calculate the tidal forces exerted by a white dwarf on a rocky planet.

2. Polytropic Structure Model

Before considering planetary collisions, we develop a structure model for the Jovian (target) planet. Here we assume that the Jovian planet consists of a rocky core of constant density surrounded by a gaseous envelope. The planet is assumed to be in hydrostatic equilibrium, and thus obeys the equations of hydrostatic equilibrium and conservation of mass,

$$\frac{dP}{dr} = -\frac{GM(r)\rho(r)}{r^2} \qquad \text{and} \qquad \frac{dM}{dr} = 4\pi r^2 \rho(r), \tag{1}$$

which can be combined into a single differential equation in terms of the pressure and density. After specifying an equation of state $P(\rho)$, the equation can be numerically integrated for the density profile. The conditions within Jovian planets lead to quite complicated equations of state, which can vary from planet to planet. At this point, there is insufficient observational and theoretical guidance to specify these equations of state. Furthermore, our goal here is to construct a relatively simple model that can be applied to the entire population of Hot Jupiters, rather than a detailed model for a single planet (with the ultimate goal of surveying the parameter space for collisions). Thus, a polytropic equation of state is adopted here, of the form

$$P = K\rho^{\Gamma} \qquad \text{where} \qquad \Gamma = 1 + 1/n, \tag{2}$$

where K is a constant, and n is the polytropic index. Here we consider a range of polytropic indices $n = 1 - 2$, but detailed models suggest that Jovian planets are characterized by indices near the lower end of this range (Burrows 2011).

Following the formulation of Chandrasekhar (1939), we define dimensionless quantities ξ and $f(\xi)$ through the relations

$$\xi = r/R, \qquad \text{and} \qquad f^n = \rho/\rho_c, \qquad \text{where} \qquad R^2 = \left(\frac{K\Gamma}{(\Gamma-1)4\pi G {\rho_c}^{2-\Gamma}}\right), \tag{3}$$

and where ρ_c is the central density, and R is a constant with units of length. With these definitions, the resulting differential equation for $f(\xi)$ becomes the Lane-Emden equation,

$$\frac{1}{\xi^2}\frac{d}{d\xi}\left(\xi^2 \frac{df}{d\xi}\right) + f^n = 0, \tag{4}$$

with the boundary conditions

$$f(\xi_c) = 1 \qquad \text{and} \qquad \left.\frac{df}{d\xi}\right|_{\xi=\xi_c} = 0, \tag{5}$$

where ξ_c denotes the radius of the planetary core.

Although polytropic stellar structure models have been used extensively (Chandrasekhar 1939; Phillips 1994), this application differs from most previous cases in two respects: First, we include the possibility of a constant density core, so that the (dimensionless) core radius ξ_c provides an additional parameter. Second, the expected values of the polytropic index are closer to $n = 1$ for giant planets, instead of the more familiar value $n = 3/2$ for degenerate stars and convective stars, or $n = 3$ for massive stars dominated by radiation pressure (Phillips 1994). The introduction of an additional parameter allows a much larger variety of planet structures to be constructed.

In terms of the dimensionless variables, the mass conservation equation is given by

$$\frac{d\mu}{d\xi} = \xi^2 f^n, \tag{6}$$

which is related to the physical enclosed mass profile $M(r)$ via

$$M(r) = 4\pi R^3 \rho_c \mu(\xi). \tag{7}$$

The total dimensionless mass of the planet is thus

$$\mu_0 = \int_0^{\xi_0} \xi^2 f^n(\xi) d\xi, \tag{8}$$

and the physical mass and radius are given by

$$M_P = 4\pi R^3 \rho_c \mu_0 \qquad \text{and} \qquad R_P = R\xi_0. \tag{9}$$

Although the planetary structure is hydrostatic and does not depend on time, orbital motion is time dependent. We thus define a dimensionless time variable

$$\tau = t/t_0 \qquad \text{where} \qquad t_0 = (4\pi G\rho_c)^{-1/2}. \tag{10}$$

The constant t_0 is identified as the free-fall time appropriate for the density at the planet center, and provides a benchmark dynamical time scale for the orbit calculations. For example, a planet with $\rho_c \approx 10$ g cm^{-3} corresponds to a time scale $t_0 \sim 6$ min.

The full set of dimensionless variables are summarized below:

$$r = R\xi, \quad \rho(r) = \rho_c f^n(\xi), \quad t = t_0\tau, \quad M(r) = 4\pi R^3 \rho_c \mu(\xi). \tag{11}$$

By introducing these dimensionless variables, the calculations are significantly simplified.

Numerical integration of equation (4) yields a dimensionless density profile, which can be converted to physical units by specifying the central density. The surface of the planet corresponds to the radius ξ_0 where the density and pressure vanish (i.e. the first zero of f). The solutions past this point are physically irrelevant and are not considered further. Solution curves of $f(\xi)$ and $\mu(\xi)$ are shown in Figure 1 for a polytropic index $n = 1$ and core radii $\xi_c = 0 - 1$. Variation of the parameters ξ_c and n lead to a range of density profiles, and upon specification of the physical planet mass and radius, different central densities and pressures, core masses, and core radii. This model thus allows us to explore a variety of planet structures. For this thesis, we vary ξ_c over a wide range, with a focus on $\xi_c = 0 - 1$ and vary the polytropic index over the range $n = 1-2$. Note that a dimensionless core radius $\xi_c = 1$ corresponds to a core mass of $M_c \approx 20 - 30 M_\oplus$, for varying n. The dimensionless radii and masses, along with the central densities, core masses, and core radii are given in Tables 1 through 3, for planets with Jovian masses and radii. The central densities obtained range from $\rho_c = 2 - 15$ g cm^{-3}, leading to central pressures $P_c \sim 100$ Mbar, in agreement with more complicated models (Militzer et al. 2008).

In general, equation (4) must be numerically integrated. However, an analytic solution exists for a polytropic index of $n = 1$, of the form

$$f(\xi) = A\frac{\cos\xi}{\xi} + B\frac{\sin\xi}{\xi}. \tag{12}$$

For a coreless polytrope, the first term must vanish to avoid divergence at the origin ($A = 0$), and the solution simplifies to

$$f(\xi) = \frac{\sin\xi}{\xi}. \tag{13}$$

For non-zero core radii, the constant A must be retained. After imposing the boundary conditions, equation (12) takes the form

$$f(\xi) = (\xi_c \cos\xi_c - \sin\xi_c)\frac{\cos\xi}{\xi} + (\xi_c \sin\xi_c + \cos\xi_c)\frac{\sin\xi}{\xi}. \tag{14}$$

Analytic expressions for the mass can be found by substituting this solution into equation (6). Doing so, we find that for the coreless polytrope,

$$\mu(\xi) = -\xi\cos\xi + \sin\xi, \tag{15}$$

and for finite core radii,

$$\mu(\xi) = \begin{cases} \frac{1}{3}\xi^3, & \text{for } \xi \le \xi_c \quad (16) \\ \frac{1}{3}{\xi_c}^3 + (\xi_c - \xi)\cos(\xi - \xi_c) + (1 + \xi_c\xi)\sin(\xi - \xi_c), & \text{for } \xi > \xi_c. \quad (17) \end{cases}$$

For a coreless polytrope, the first zero occurs at $\xi_0 = \pi$, but for finite core radii the first zero ξ_0 must be determined by solving a transcendental equation (14). Although the coreless polytrope is a relatively good model for planets with small cores like Jupiter, it is less accurate for the extrasolar giant planets with massive cores. Nonetheless, it still serves as a reasonable approximation and the simple analytic forms for the density and mass profiles are convenient for later calculations, and are used extensively in this work.

For a polytrope of fixed index n and core radius ξ_c, the model provides a two parameter family of solutions, where the parameters are the central density ρ_c and the coefficient K in the equation of state. This coefficient K depends on the physics of the planetary interior and can take a range of values. Specifying both ρ_c and K results in a prediction for the planetary mass M_P and radius R_P. Alternatively, specifying M_P and R_P results in a prediction for ρ_c and K. For any observed planet with measured mass and radius, we can calculate the central density and pressure, thereby allowing us to compare the model predictions with observations. The central pressures and densities have been calculated for Jupiter and Saturn in Figure 2, along with the central properties of the transiting exoplanets[1]. These central properties are poorly constrained because the planet interiors are impossible to directly observe and difficult to recreate experimentally. The central pressure of Jupiter is thought to lie in the range $P_c = 10 - 100$ Mbar, with estimates around 70 Mbar, and that of Saturn a bit lower, perhaps 40 Mbar (Saumon & Guillot 2004). More detailed knowledge of these conditions requires a reliable equation of state for hydrogen at high pressures, especially in the transition to metallic hydrogen. This poses significant experimental and theoretical challenges, and many uncertainties regarding the interiors of gas giants thus remain; a description of these difficulties is given by Hubbard et al. (2002). However, the broad constraints listed above are in rough agreement with our predicted model values for Jupiter and Saturn.

The central pressures, although somewhat uncertain, follow the relation

$$P_c = \mathcal{F}\frac{GM_P^2}{\pi R_P^4} = K\rho_c, \tag{18}$$

where this equation follows from the condition of hydrostatic equilibrium and the polytropic equation of state. The dimensionless factor $\mathcal{F}$ is expected to be of order unity. In terms of the model parameters, $\mathcal{F}$ can be written in the form

$$\mathcal{F} = \frac{\xi_0^4}{4\mu_0^2(n+1)}. \tag{19}$$

As an additional consistency check, this factor has been calculated, and is shown in Figure 3 as a function of the core radius for the polytropic indices $n = 1, 1.5$, and 2. The values of $\mathcal{F}$

[1]All observational data used in this thesis was taken from www.exoplanet.eu on March 4, 2012.

are indeed of the order unity (which indicates that the model predictions are reasonable), in the range $\mathcal{F} \approx 1 - 5$. For an $n = 1$ polytrope with no core, $\xi_0 = \mu_0 = \pi$, so that $\mathcal{F} = \pi^2/8$.

One simplification introduced herein is that the outer atmosphere of the Jovian planet has been neglected. Detailed planetary structure models include separate models for the outer atmosphere, which are incorporated into the full model by demanding that the pressure and density are continuous at the boundary between the outer and inner atmospheres. In the treatment of this problem, we have neglected this detail, because the depths of the outer atmospheres are small compared to the planetary radii and will not affect the collisional dynamics. To ensure that our polytropic model predicts structures that are consistent with this fact, temperature profiles have been calculated for the sample of exoplanets and compared with the effective temperatures determined from observations. If this model is robust, the predicted depth of the atmosphere should be small compared to the planet radius. More specifically, the depth of the atmosphere d should satisfy the relation

$$d = \gamma R_P \qquad \text{with} \qquad \gamma << 1, \tag{20}$$

where the atmosphere depth d is measured from the surface of the planet.

Since the polytropic relation does not involve the temperature, an additional equation of state is required; here we adopt the ideal gas law. Although the ideal gas law is clearly invalid deep in the planet interior, near the surface this equation of state is correct to within an order of magnitude. The effective temperatures of the observed planets can be calculated via

$$T_P = (1 - \alpha)^{1/4} \left(\frac{R_*}{2a} \right)^{1/2} T_*, \tag{21}$$

where the stellar radius R_*, surface temperature T_*, and planet semi-major axis a are measured quantities, and α is the albedo of the planet. There is some uncertainty in the effective temperatures due to uncertainties in the planet albedos. Furthermore, these albedos vary from planet to planet (Sudarsky et al. 2000). For this calculation, we adopt an albedo of zero for the entire sample, which yields an upper limit on the effective temperature.

An example of the predicted temperature profile for one of the observed transiting planets (based on the polytropic model and the ideal gas law) is given in Figure 4a (solid curve), along with the effective temperature predicted by equation (21) (dashed line). The point where these curves intersect indicates the predicted atmosphere depth d. Note that by assuming albedos of zero we are working with the maximum possible effective temperatures. Since the actual temperatures are probably somewhat lower, the point of intersection will be shifted to larger radii, which means that the depth of the atmosphere will decrease. The distribution of predicted atmospheric depths as a fraction of the planetary radius shown in

Figure 4b thus indicates the worst-case scenario; the actual atmospheric depths are probably even lower. Even in this case, almost all of the planets have atmospheric depths $d \leq 0.1 R_P$.

The previous consistency checks indicate that for the purposes of this work, the polytropic model developed herein can be safely applied to the observed sample of Hot Jupiters. In addition to this problem, the model can be used for future theoretical problems involving giant planet structure.

3. Orbital Trajectories

In this section we solve the equations of motion for a rocky planet as it falls into a gaseous giant planet. In this setting, we assume that the Hot Jupiter has completed its inward migration and entered into a stable orbit close to its star, with semi-major axis $a < 0.1$ AU. Rocky planets migrate in later and have a high probability of colliding with the Hot Jupiter, provided that their orbital eccentricity is not overly damped (Ketchum et al. 2011b). At the start of these integrations, the rocky planet already lies well within the Hill sphere of the Jovian planet so that the gravitational field of the host star can be neglected. The system thus consists of a Jovian planet with fixed mass $M_P = 1 M_J$, and a smaller rocky planet $m_{\rm p} << M_P$. To first approximation, the system can be treated as a one-body problem, with the origin of the coordinate system placed at the center of the Jovian planet. As the rocky planet orbits within the gaseous envelope of the Jovian planet, it experiences the usual gravitational force, and a frictional (ram pressure) force, so that the equation of motion is given by

$$\ddot{\mathbf{r}} = \frac{-GM(r)}{r^2}\hat{r} - \frac{\rho(r) v^2 \Sigma_{\rm p}}{m_{\rm p}}\hat{v}, \tag{22}$$

where $\Sigma_{\rm p} \sim \pi {r_{\rm p}}^2$ is the effective cross sectional area of the rocky planet (for determining ram pressure forces). Substituting the definitions from equation (11), we obtain

$$\frac{\ddot{\mathbf{r}}}{R} = \frac{-\mu(\xi)}{\xi^2}\hat{r} - \alpha f^n v^2 \hat{v}, \tag{23}$$

where v is now the dimensionless speed (in units of R/t_0), and where time derivatives are performed with respect to the dimensionless time τ (from equation [10]). We have introduced a dimensionless friction coefficient α, defined by

$$\alpha \equiv \frac{{\xi_0}^2}{4\pi\mu_0}\left(\frac{M_P}{m_{\rm p}}\right)\left(\frac{{\Sigma_{\rm p}}^2}{{R_P}^2}\right), \tag{24}$$

which depends on the masses and radii of both planets, as well as the polytrope characteristics. Here we consider rocky planets with masses $m_{\rm p} = 0.1 - 20 M_\oplus$. For a typical mean

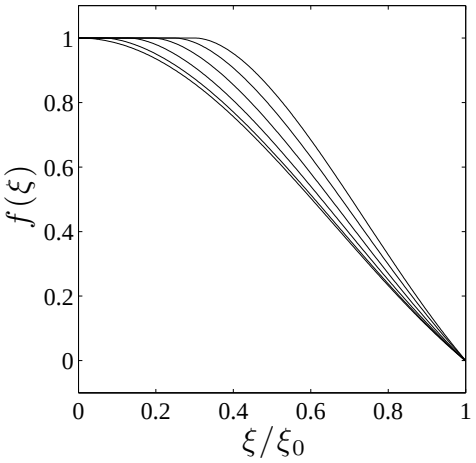

(a)

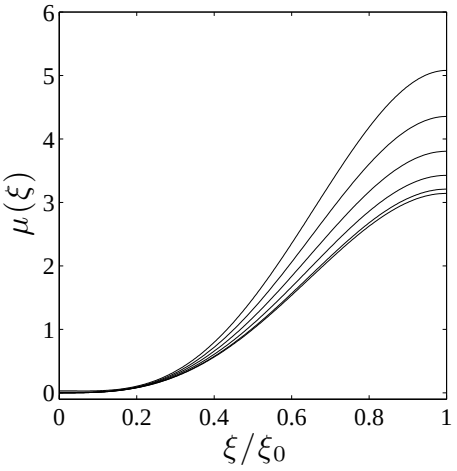

(b)

Fig. 1.— Density and mass profiles $f(\xi)$ and $\mu(\xi)$ for $n = 1$ polytropic models with a collection of core masses. Each curve corresponds to a different core radius from $\xi_c = 0$ (bottom) to $\xi_c = 1$ (top). For the largest core radius $\xi_c = 1$ shown here, the core makes up $\sim 6.6\%$ of the mass (e.g., the core would have mass $m_c \sim 21 M_\oplus$ for a giant planet mass $M_P = 1 M_J$). Here the radial coordinate has been scaled by the dimensionless planetary radius ξ_0, but the value of ξ_0 changes with both polytropic index and core radius. See Tables 1 through 3 for numerical values of ξ_0 as a function of the core radius.

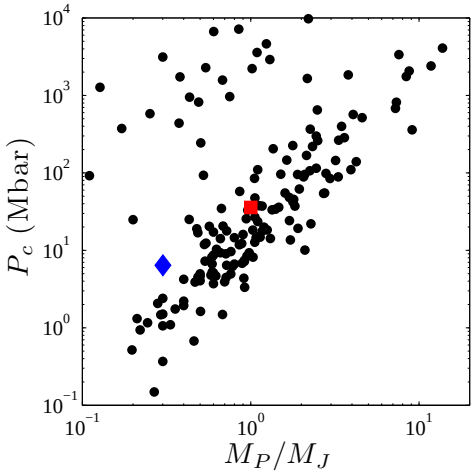

(a)

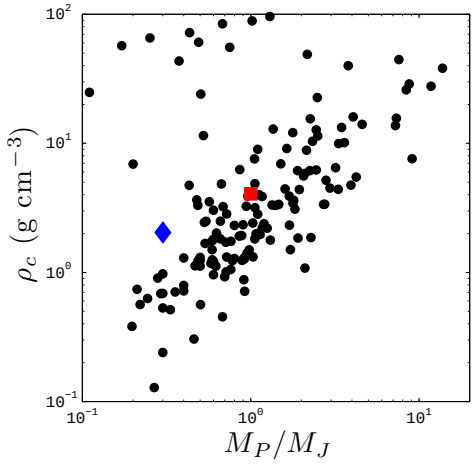

(b)

Fig. 2.— Predicted central pressures and densities as a function of planet mass for Jupiter (red square) and Saturn (blue diamond), along with the sample of transiting exoplanets (black circles), where only planets with masses $0.1 < M_P < 20 M_J$ are shown. Model parameters $n = 1$ and $\xi_c = 0$. The planets generally fall along a well-defined band, with most of the central pressures within the expected range $1 < P_c < 100$ Mbar. The objects at the upper end of this band are entering the brown dwarf regime, and thus have significantly higher central pressures and densities. The planets above this band with high central densities, in the upper left hand corner, correspond to superearths (with rocky compositions), and thus are not appropriate for this model.

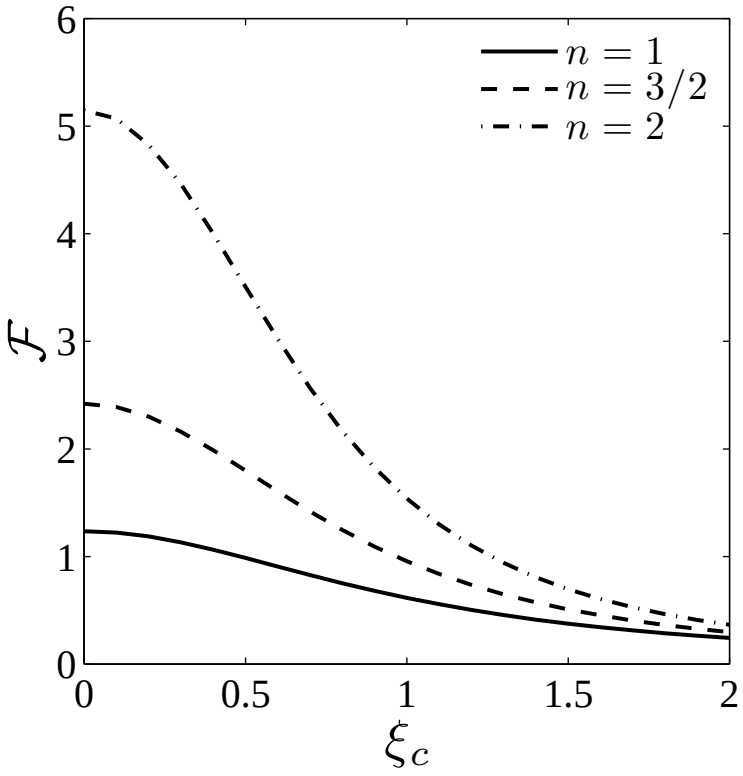

Fig. 3.— Dimensionless factor $\mathcal{F}$ from equation (19). Polytropic index $n = 1$ (solid curve), $n = 3/2$ (dashed curve), and $n = 2$ (dashed-dot curve). $\mathcal{F}$ increases with polytropic index for planets with small core masses, but becomes nearly independent of n as the core mass increases. In general, $\mathcal{F}$ is of order unity, which is consistent with equation (18) and indicates that the model is reasonable. For the $n = 1$ polytrope with no core, $\mathcal{F} = \pi^2/8$.

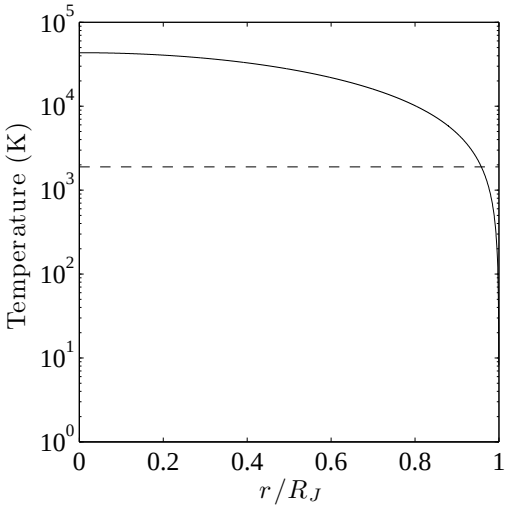

(a)

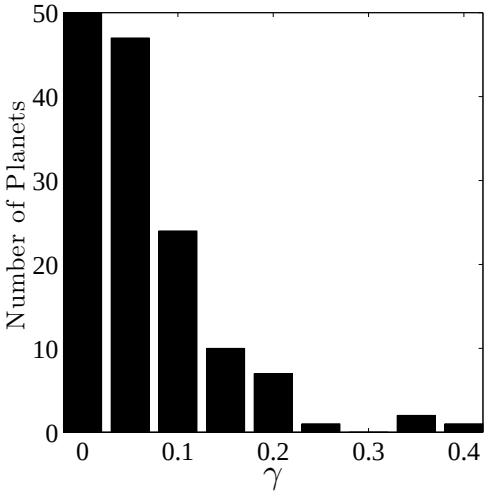

(b)

Fig. 4.— (a): Example of the predicted temperature profile for an observed Hot Jupiter (solid curve). The dashed horizontal line indicates the effective temperature calculated from observations, assuming an albedo $\alpha = 0$. The point where the solid and dashed curves intersect gives an indication of the predicted depth d of the atmosphere. This calculation was performed for the entire sample of transiting extrasolar planets, and the distribution of the atmospheric depths is shown in (b), where $\gamma = d/R_P$. Most of the predicted depths are small, with $\gamma \leq 0.1$ for most planets.

density $\rho_p = 5.5$ g cm^{-3} for the rocky planet, and for $M_P = 1 M_J$ and $R_P = 1 R_J$, the corresponding values of α fall in the range $\alpha \approx 0.5 - 5$. Note that Jovian planets with inflated radii have lower values of α and provide less friction.

The parameter space is composed of five variables: The impact parameter, initial velocity, friction coefficient α, and the polytrope variables ξ_c and n. Once these parameters are specified, the equation of motion (23) can be numerically integrated. The integration scheme used in these calculations is a fourth-order Runge-Kutta algorithm (e.g., Press et al. 1992).

3.1. Orbits of Rocky Planets Within Jovian Planets

To begin, we consider the simple case of a coreless Jovian planet ($\xi_c = 0$), and adopt a polytropic index $n = 1$. By fixing the polytropic index and core radius, the number of free parameters is reduced to three. Starting with a simplified model allows us to perform a preliminary survey of the parameter space, identify the basic qualitative behavior of the system, and determine the appropriate follow-up calculations. The goal is to understand the dynamics of test particles within a polytropic potential, and determine the implications in the context of planet collisions.

The starting conditions are defined as follows: All calculations are started with the incoming rocky planets located at the surface of the Jovian planet, travelling in the $-\hat{y}$ direction. In dimensionless coordinates, the rocky planet has the initial position (x_0, y_0), where x_0 is identified as the impact parameter. The starting coordinates thus obey the constraint

$$x_0^2 + y_0^2 = \xi_0^2. \tag{25}$$

Here we explore the full range of impact parameters $0 \leq x_0 \leq \xi_0$, and consider rocky planet masses $m_{\rm p} = 0.1$, 1, and 10 $M_\oplus$. If the Jovian planet has the mass and radius of Jupiter, these values correspond to friction coefficients $\alpha \approx 5, 3$ and 1. We also consider a very wide range of initial velocities in these preliminary integrations to determine the penetration velocity (see below), although dynamical simulations indicate that the expected initial velocities lie in the range $v_0 = 40 - 150$ km s^{-1} (Ketchum et al. 2011b). Examples of typical trajectories are shown in Figure 5 for an initial velocity $v_0 = 40$ km s^{-1}, and all three rocky planet masses. As the planets spiral inward, the orbits of large planets remain relatively circular, while the orbits of small planets become highly elliptical. In general, the bodies continuously spiral inward and approach the origin asymptotically (see Appendix B for a discussion on the dynamical behavior in the limit of small radial coordinate ξ).

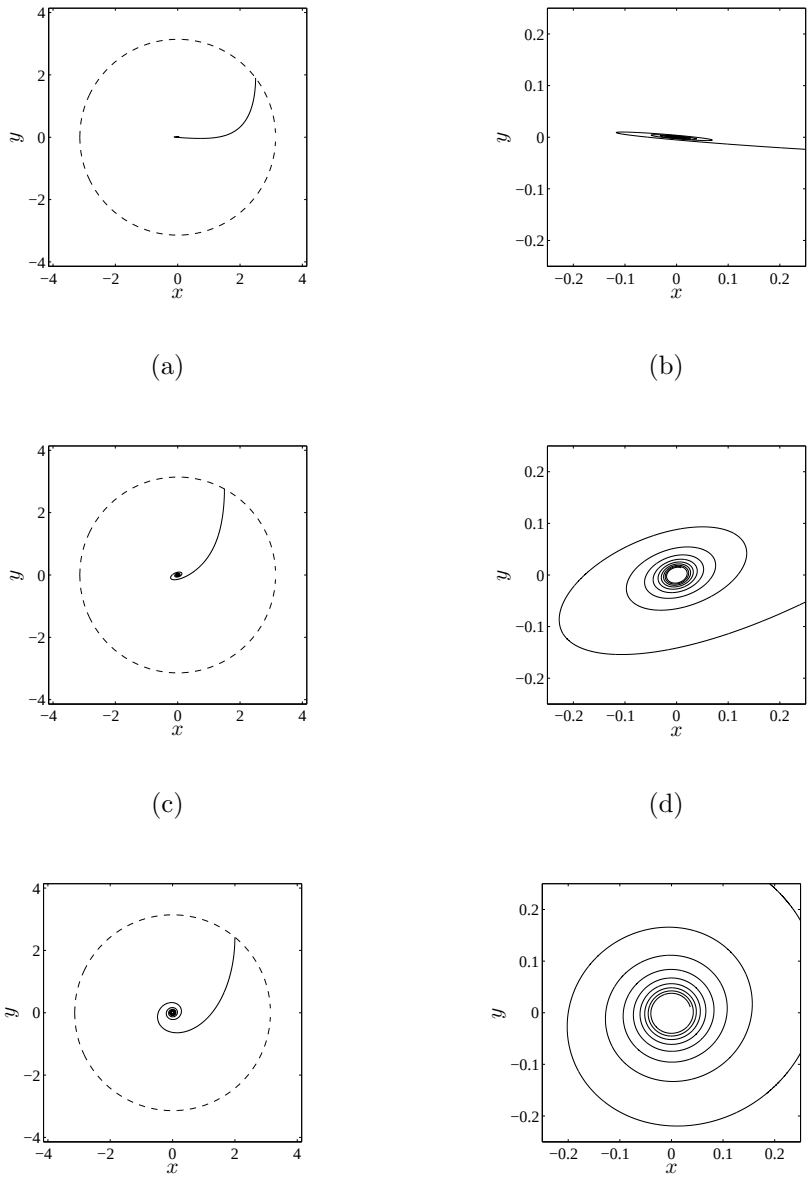

Fig. 5.— Orbits within coreless Jovian planets with polytropic index $n = 1$, initial velocity $v_0 = 40$ km s^{-1}, and rocky planet masses $m_{\rm p} = 0.1 M_\oplus$ (top), $1 M_\oplus$ (middle), and $10 M_\oplus$ (bottom). The panels on the left show the full planetary view, whereas the panels on the right show the same orbits on a smaller spacial scale. Dashed circle indicates the Jovian planet surface. The planets continuously spiral inward and approach the origin slowly; see Appendix B for a discussion of this dynamical behavior.

There are two possible outcomes of these orbits: Either the rocky planet is captured and spirals inward, or it passes through the gaseous planet and retains enough kinetic energy to escape. For an incoming rocky planet with impact parameter x_0, we can determine the initial velocity necessary for the rocky planet to avoid permanent capture. More specifically, the critical condition for penetration requires that the rocky planet initially has enough kinetic energy so that it passes through the gaseous planet and leaves the surface traveling outward at the escape speed. This penetration speed is denoted here as $v_{\rm pen}$ and is a function of the impact parameter x_0. For a given impact speed, incoming rocky planets will be captured for all impact parameters $x_0 < x_*$, where the maximum impact parameter defines the effective capture cross section $\sigma(v_0) = \pi x_*^2$. Here we calculate the required penetration speeds numerically using the above formulation, and compare with the following analytic estimation for $v_{\rm pen}(x_0)$.

We begin the analytic approximation by deriving relations for the velocity and radial coordinate as functions of time. To leading order, gravity can be neglected, and the equation of motion simplifies to the form

$$\frac{d\mathbf{v}}{d\tau} = -\alpha f^n v^2 \hat{v} = -\alpha f^n v(\dot{x}\hat{x} + \dot{y}\hat{y}), \tag{26}$$

where all variables are dimensionless. For the cases of interest here, where the rocky planet is not captured, the path of the rocky planet through the Jovian planet can be approximated as a straight line. Since we have defined the starting velocity to be in the $-\hat{y}$ direction, we can set $\dot{x} \approx 0$, and $v = \dot{y}$. With these simplifications, equation (26) becomes

$$\frac{dv}{d\tau} = -\beta v^2, \qquad \beta \equiv \alpha \langle f^n \rangle, \tag{27}$$

where we have approximated $f^n = \langle f^n \rangle$. This differential equation is easily integrated. Applying the boundary condition $v = v_0$ at time $\tau = 0$ (and recall the constraint equation [25]), we obtain

$$v = \frac{dy}{d\tau} = \frac{v_0}{1 + \beta v_0 \tau}. \tag{28}$$

Integrating equation (28) for $y(\tau)$, yields the solution

$$y - y_0 = \beta^{-1} \ln(1 + v_0 \beta \tau), \tag{29}$$

and upon substitution into equation (28)

$$v = v_0 e^{-\beta(y - y_0)}. \tag{30}$$

In order for the rocky planet to avoid capture, its speed must exceed the escape speed ($v > v_{\rm esc}$) at the location $y = -y_0$, where $v_{\rm esc} = (2\mu_0/\xi_0)^{1/2}$. The minimum initial speed $v_{\rm pen}$

required for penetration is thus given by the condition

$$v_{\rm esc} = v_{\rm pen} e^{-2\beta|y_0|} \qquad \text{or} \qquad \mathrm{v_{pen}} = \mathrm{v_{esc}} \mathrm{e}^{2\beta|\mathrm{y_0}|}. \tag{31}$$

Notice that it is possible for rocky planets to completely penetrate the Jovian planet but leave the surface with $v < v_{\rm esc}$, and thus remain gravitationally bound. Figure 6 shows an example of such a trajectory. Equation (31) gives the condition for the rocky planet to penetrate *and* remain unbound.

Next we find the dependence of the penetration speed $v_{\rm pen}$ on the impact parameter x_0. Here we estimate the average density by approximating the density profile of the Jovian planet as a Gaussian function, where the peak is a function of the impact parameter. For head-on collisions, with $x_0 = 0$, we assume $\langle f^n \rangle \approx 1/2$. The constant β is therefore

$$\beta = \frac{1}{2} \alpha \exp\left[-\gamma {x_0}^2\right], \tag{32}$$

where we have introduced an unspecified parameter γ. We find that the best agreement with numerical results is obtained using $\gamma = 1/4$. Equations (31) and (32) together yield a simple relation between the initial velocity and the impact parameter. In the limiting case of grazing collisions, where $x_0 = \xi_0$ and $y_0 = 0$, $v_{\rm pen} = v_{\rm esc}$. On the other hand, for head-on collisions where $x_0 = 0$ and $y_0 = \xi_0$, the penetration speed attains its maximum value $v_{\rm pen} = v_{\rm esc} \exp\left[\alpha \xi_0\right]$. Typical values of α and ξ_0 are ~ 3, so that the exponential factor is large and $v_{\rm pen} >> v_{\rm esc}$.

The above derivation assumes that $\langle f^n \rangle \approx 1/2$ for impact parameter $x_0 = 0$. For the particular case where $n = 1$ with no central core, we can directly test this approximation using equation (13):

$$\langle f^n \rangle = \langle f \rangle = \frac{1}{\pi} \int_0^\pi \frac{\sin \xi}{\xi} d\xi = \frac{1}{\pi} \mathrm{Si}(\pi), \tag{33}$$

where $\mathrm{Si}(x)$ is the sine integral (Abramowitz & Stegun 1970), which has the known value $\mathrm{Si}(\pi) \approx 1.85194$, so that $\langle f \rangle \approx 0.5895$. Thus, the approximation is reasonable.

The analytic approximation is plotted along with numerical results in Figure 7 using a value of $\gamma = 1/4$ and for a friction parameter $\alpha = 3$. The best agreement between the numerical and analytic results occurs for large impact parameters because the assumption of constant density is more accurate far from the center of the planet; even for small impact parameters however, the results agree within a factor of two. These calculations show that enormous starting velocities are required for penetration when the collisions are head-on, i.e., $v_{\rm pen} \sim 10^6$ km s^{-1}. For intermediate impact parameters $x_0 \sim \xi_0/2$, penetration still requires $v_{\rm pen} \sim 1000$ km s^{-1}. As a result, the cross section for capture is large. For the expected impact speeds $v_0 = 40 - 150$ km s^{-1}, rocky planets will penetrate the polytrope only for

impact parameters comparable to the radius of the Jovian planet, roughly $x_0 \gtrsim 0.8\xi_0 = x_*$. For high-speed rocky planets with $v_0 > 100$ km s^{-1}, the effective target area (cross section for capture) of the Jovian planet is reduced slightly, but the critical impact parameter x_* remains above $\sim 70\%$ of the planetary radius.

We now consider the general case where rocky planets collide with Jovian planets containing central cores, and begin by choosing a standard (dimensionless) core radius $\xi_c = 1$. Depending on the polytropic index, this core radius spans $\sim 20-30\%$ of the giant planet radius, and encloses a mass $M_c \approx 20-30 M_\oplus$. Here we use three polytropic indices ($n = 1.0, 1.5,$ and 2.0), four terrestrial planet masses ($m_{\rm p} = 0.1$, 1 ,10, and 20 $M_\oplus$), and the full range of impact parameters $x_0 = 0 - \xi_c$, and where the initial velocities span the range $v_0 = 30 - 150$ km s^{-1}. The resulting trajectories, including profiles of energy dissipation and the velocities upon impact with the core, are nearly independent of the polytropic index. Since similar results were obtained for all polytropic indices, only the results for the $n = 1$ polytrope are shown here. Figure 8 shows the trajectories for rocky planets with initial speeds $v_0 = 70$ km s^{-1} and varying impact parameter.

We note that the presence of a central core has little effect on the ability of a rocky planet to penetrate the Jovian planet and avoid capture. In fact, the presence of a core introduces a minimum capture cross section, since incoming projectiles cannot pass through the Jovian planet when the impact parameter is less than the core radius. As a result, the results depicted in Figure 7 remain valid; only planets with large impact parameters ($\xi_0 \gtrsim 0.8\xi_0$), or incredibly high initial speeds ($v_0 > 1000$ km s^{-1}) are able to escape.

3.2. Energy Dissipation

During each inward trajectory, energy is dissipated through the action of frictional forces. Figures 9 and 10 show the rocky planet's total energy (kinetic and potential) as a function of radial distance, measured from the center of the giant planet, where each curve represents a unique trajectory. For giant planets with the mass and radius of Jupiter, most of the energy is dissipated in the outer atmosphere ($r/R_P > 0.5$). When the projectile planet strikes the core, its motion is arrested and any remaining kinetic energy is converted into heat. The amount of energy upon impact with the core thus determines the extent of the core deformation, as well as the amount of energy available for long-term heating. This quantity can range from less than 1% to almost 40% of the initial energy, depending on the rocky planet mass.

The planet velocities and their corresponding kinetic energies at the moment of impact

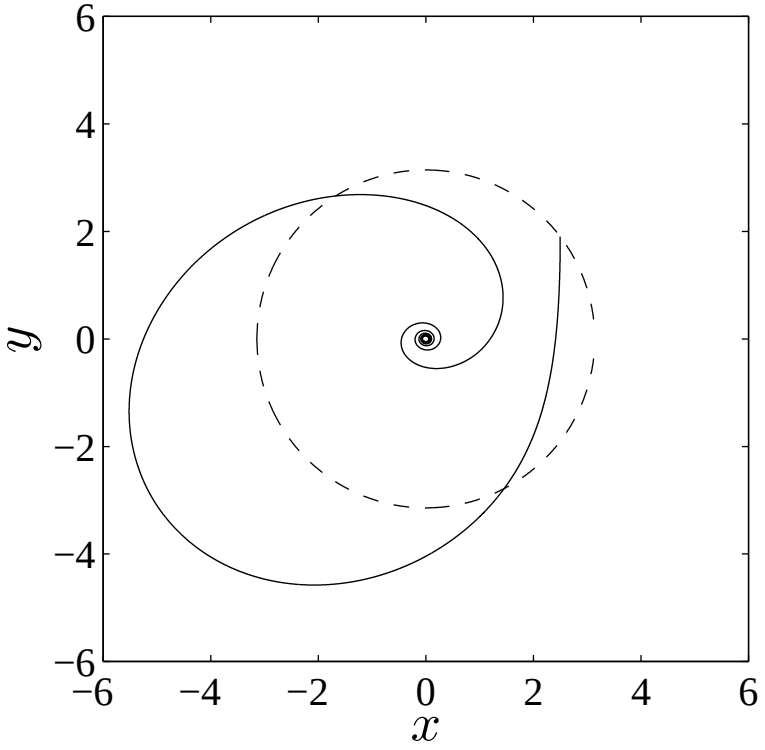

Fig. 6.— Example of a trajectory where the rocky planet completely penetrates the Jovian planet, but emerges from the far surface with speed $v < v_{\rm esc}$. Such planets remain gravitationally bound and eventually spiral inward. Although this situation can lead to interesting dynamics, the cases of interest here are the planets that remain unbound, with speed $v \geq v_{\rm esc}$ when they emerge from the far surface (in order to determine the capture cross section). In this trajectory, the rocky planet has mass $m_{\rm p} = 10 M_\oplus$ and initial speed $v_0 = 100$ km s^{-1}.

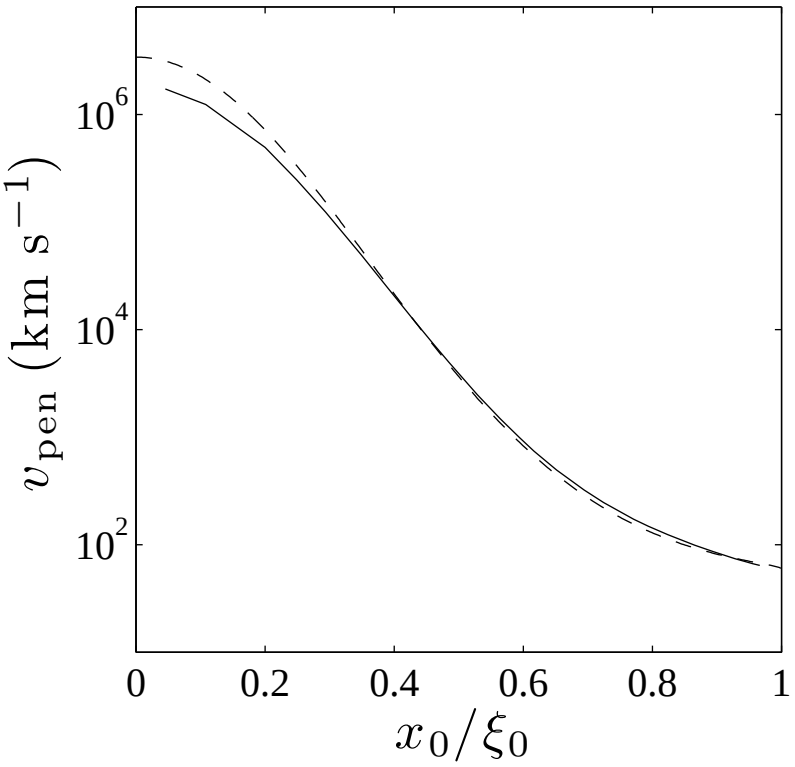

Fig. 7.— Penetration velocity as a function of impact parameter. The velocity $v_{\rm pen}$ is the initial velocity needed for the rocky planet to pass through the gaseous planet, emerge from the far side, and remain uncaptured. The impact parameter x_0 is given as a fraction of the planetary radius. The friction coefficient used in these calculations is $\alpha = 3$, which corresponds to a rocky planet mass $m_{\rm p} \sim 1 M_\oplus$ for a Jovian planet with the mass and radius of Jupiter. The solid curve indicates the numerical results and the dashed curve indicates the analytic approximation. Note that the approximation works well over the entire range of impact parameters, but the best agreement occurs for large impact parameters, because the approximation of constant density is most accurate in the outer regions of the envelope.

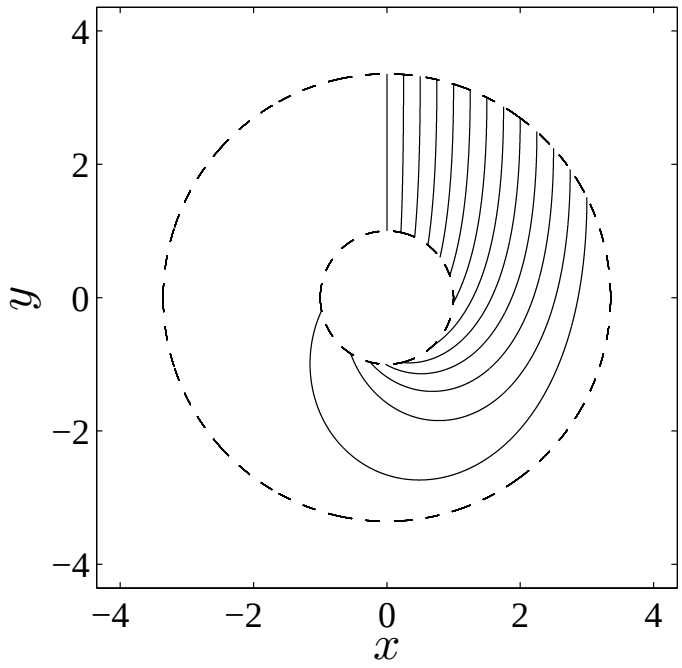

Fig. 8.— Trajectories with constant initial velocity $v_0 = 70$ km s^{-1} and varying impact parameters. The outer dashed circle marks the location of the surface of the Jovian planet; the inner dashed circle indicates the core radius $\xi_c = 1$. The Jovian planet has mass $M_P = 1M_J$, radius $R_P = 1R_J$, and polytropic index $n = 1$. For impact parameters $x_0 \lesssim \xi_c$, the projectile planets collide directly with the core, but beyond this critical impact parameter, the path length can increase considerably. The presence of a core does not significantly affect the capture cross section, and thus the results for the coreless polytrope still apply.

with the core are shown in Figure 11, as a function of both the initial velocity and impact parameter. The impact velocities v_f vary from $10 - 75$ km s^{-1}, leading to impact energies $E_f \approx 10^{38} - 10^{42}$ ergs, where this range is strongly dependent upon the rocky planet mass. Planets with mass $m_{\rm p} \leq 1 M_{\oplus}$ show very little spread in the final velocity for the entire set of impact parameters and initial velocities. This result can be understood in terms of the nature of the frictional force ($F_f \sim \rho v^2$) and the strength of the friction coefficient α. Planets with the highest velocities experience the highest level of damping, and their speeds are quickly diminished. Furthermore, the impact parameter determines the average density encountered by the orbiting planets. Although the average density is lower for planets incident at large impact parameters, these planets must travel farther distances before being accreted onto the core, and are thus subjected to damping forces acting over larger distances. These effects are the most pronounced for low-mass planets, since they experience the greatest frictional forces relative to gravitational forces. Planets with masses $m_{\rm p} \gtrsim 1 M_{\oplus}$ are subjected to relatively less friction and are more sensitive to variations in the initial velocity and impact parameter. Planets incident at small impact parameters (roughly $x_0 \leq \xi_c$) collide directly with the core and travel shorter distances. These planets thus experience less damping, and retain a significant amount of energy upon impact with the core. Incoming planets with sufficiently large impact parameters do not collide directly with the core, but rather gradually spiral inward, and can enter into highly elliptical orbits. The orbital path length increases substantially for impact parameters larger than a critical value, and the amount of energy deposited at the core decreases accordingly. For the regime of parameter space considered here, this critical impact parameter is roughly $x_0 = 0.4 R_P$. Finally, notice that the curves in Figure 11 do not extend beyond $x_0 \approx 0.9 R_P$; for collisions with the largest impact parameters, the rocky planet does not remain bound and hence does not strike the core.

In the calculations presented so far, the mass and radius of the Jovian planet were those of Jupiter. However, since many of the Hot Jupiters are inflated relative to expectations, larger radii (for the same mass) must also be explored, roughly $R_P \approx 1.2 R_J$ for a mass $M_P = 1 M_J$ (Laughlin et al. 2011). In addition, the radii of young gaseous giant planets—before they contract and cool—are even larger than those of mature planets (Burrows et al. 1997). To bracket the possibilities, the previous calculations were repeated for a Jovian planet with mass $M_P = 1 M_J$, but with a larger radius $R_P = 2 R_J$, leading to a lower mean density of only $\langle \rho \rangle \sim 0.1$ g cm^{-3}, ten times lower than the mean density of Jupiter. These results are presented in Figures 13, 14, and 15. Compared to the previous case with $R_P = 1 R_J$, the impact energies are larger by an order of magnitude. Notice also that the impact velocity and energy curves do not extend beyond impact parameters $x_0 \approx 0.7 R_P$ because the rocky planets pass through the Jovian planet more easily and escape.

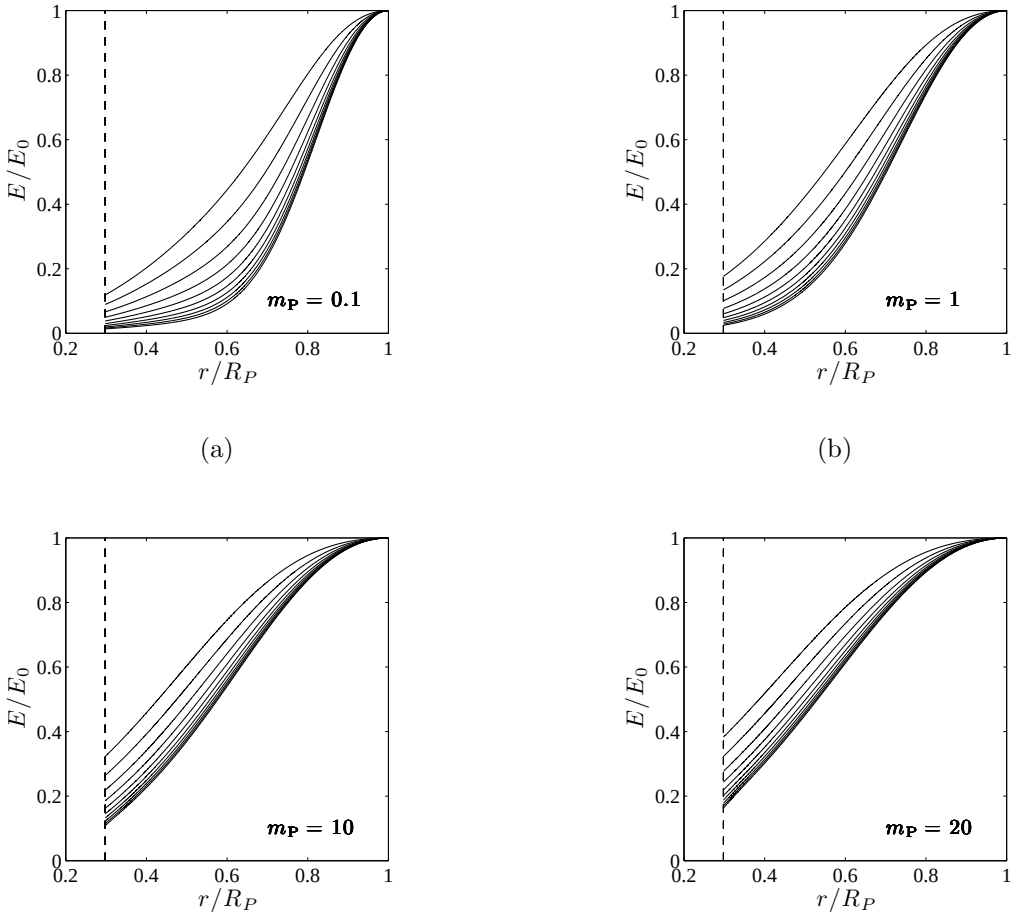

Fig. 9.— Fraction of the total energy of the rocky planet as a function of radial distance for varying initial velocities $v_0 = 30 - 150$ km s^{-1} and impact parameters $x_0 = 1$. Each curve represents a unique trajectory. Rocky planet masses (a): 0.1, (b): 1, (c): 10, and (d): 20 $M_\oplus$. Polytropic index $n = 1$, Jovian planet mass $M_P = 1 M_J$ and radius $R_P = 1 R_J$. The dashed line indicates the core radius. Energy is dissipated efficiently by friction forces, especially for the lower mass planets, and at the core-envelope boundary the energy fraction $E/E_0 \sim 0.2$ in most cases.

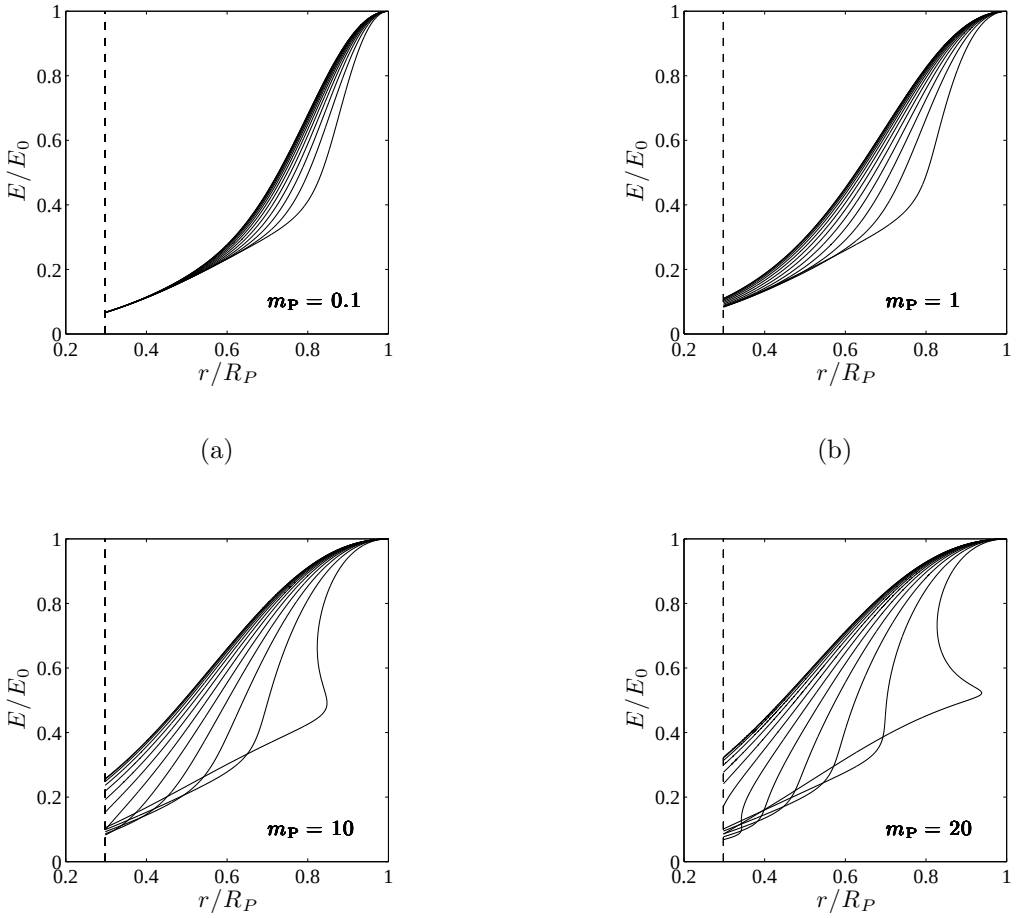

(a) (b)

(c) (d)

Fig. 10.— Fraction of the total energy of the rocky planet as a function of radial distance for varying impact parameters $0 \leq x_0 < \xi_0$, where x_0 increases from top to bottom, and initial velocity $v_0 = 80$ km s^{-1}. Rocky planet masses (a): 0.1, (b): 1, (c): 10, and (d): 20 $M_\oplus$. Polytropic index $n = 1.0$, Jovian planet mass $M_P = 1 M_J$ and radius $R_P = 1 R_J$. The dashed line indicates the core radius. Notice that for high mass planets incident at large impact parameters, the energy fraction can take multiple values for a single radius, as the rocky planet passes through multiple turning points.

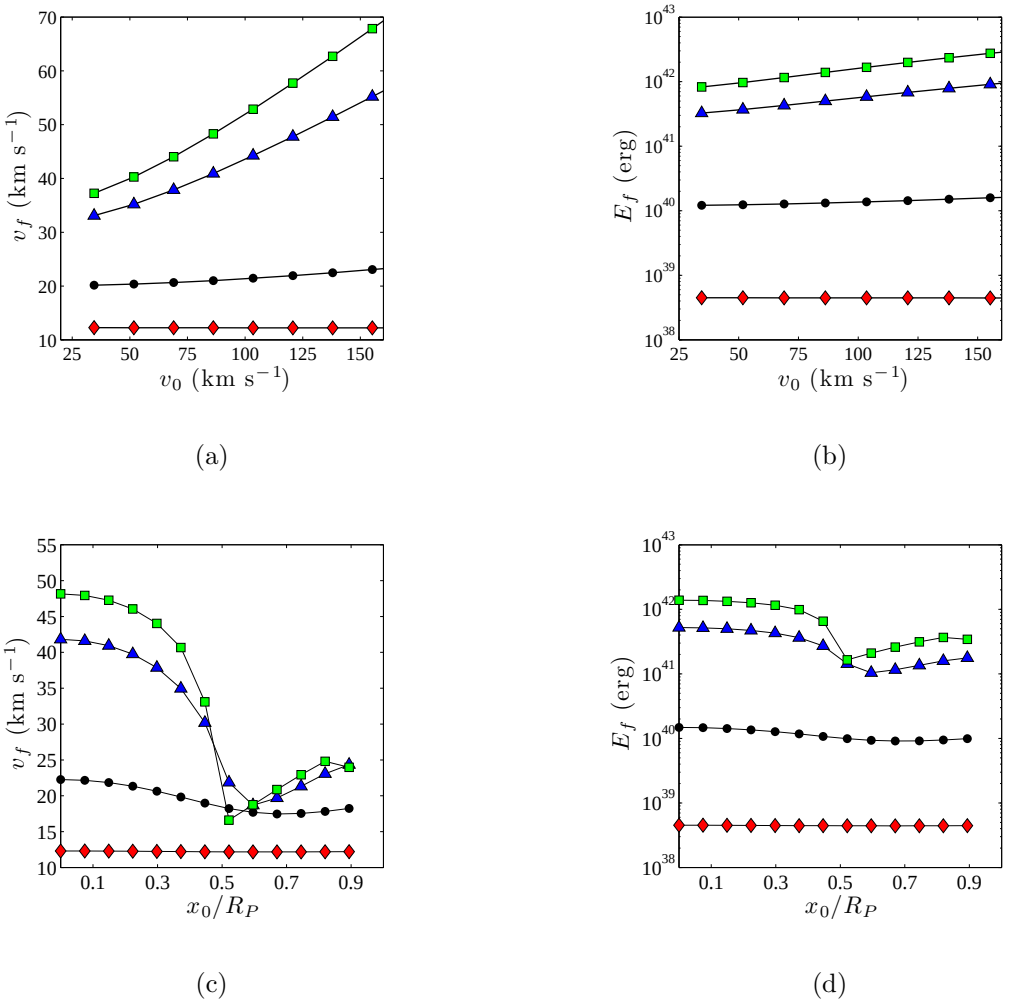

Fig. 11.— Rocky planet final velocities v_f upon impact with the core, and the corresponding kinetic energy as a function of initial velocity (top), and impact parameter (bottom), where the initial velocity is defined at the point where the rocky planet enters the atmosphere of the Jovian planet. Rocky planet mass $m_{\rm p} = 0.1M_\oplus$ (red diamonds); $m_{\rm p} = 1M_\oplus$ (black dots); $m_{\rm p} = 10M_\oplus$ (blue triangles); $m_{\rm p} = 20M_\oplus$ (green squares). The Jovian planet has mass $M_P = 1M_J$, radius $R_P = 1R_J$, polytropic index $n = 1$, and dimensionless core radius $\xi_c = 1$. The final velocity for rocky planets with lower masses is nearly independent of initial velocity and impact parameter, but can vary for planets with higher masses.

As shown in Figure 14, for sufficiently large impact parameters the energy fraction E/E_0 can take on multiple values for a given radius; on the other hand, the radius is a single-valued function of the energy. This complication arises for orbits that reach an inner turning point ($\dot{r} = 0$) and reverse course as they spiral inward (e.g., see the orbit with the largest impact parameter in Figure 8, and many of the trajectories in Figure 12). The orbits displaying the most turning points are those for projectile planets with larger masses and/or target planets with lower density. The energy fraction curves show the most structure in these cases (e.g., Figure 14c and 14d).

Another way to illustrate the effects of inflated Jovian planet radii on these orbits is to plot the energy fraction and impact energy E_f as a function of the radius of the giant planet. Figure 16 shows the energy fraction E/E_0 for Jovian planet radii $R_P = 0.7 - 2.1 R_J$, rocky planet mass $m_{\rm p} = 10 M_\oplus$, impact parameter $x_0 = 0$, and initial speed $v_0 = 50$ km s^{-1}. Figure 17 shows the impact energy for same initial velocity and impact parameter, and all four rocky planet masses. The kinetic energy E_f remaining when the rocky planet strikes the core is a smoothly increasing function of the Jovian planet radius. To leading order, the four curves in Figure 17 have nearly the same shape, so that they are scaled by the mass of the rocky planet. The starting energy for the 1 $M_\oplus$ planet is 7.5×10^{40} erg; for collisions with Jovian planets with $R_P = 2 R_J$, the impact energy is about two thirds of this starting value.

This difference in the energy dissipation between Jovian planets with different radii is remarkable. The planets with inflated radii tend to dissipate far less energy in their outer envelopes, and the percentage of the initial energy remaining when the impacting planets reach the core can be as high as 70%. Note that this percentage represents the fraction of the rocky planet's total energy (kinetic and potential) at the surface of the Jovian planet. If we examine purely the kinetic energy, we find that the energy dissipation in the outer regions is low enough that the kinetic energy can actually increase during the inward trajectory, as the rocky planet travels deeper into the potential well of the giant planet.

The consequences of these collisions differ greatly for young Jovian planets with low densities and mature planets with higher densities. Mature planets are able to dissipate much more energy near the surface, where heat is transported efficiently by radiation. In such cases, the energy of the impact is expected to radiate away quickly, and the structure of the giant planet should recover on short time scales. On the other hand, young planets with large radii tend to dissipate very little energy in the radiative zones, and the majority of the impact energy is delivered to the core, where it becomes trapped and is available for long-term heating. The evolutionary stage of the Jovian planet is therefore an important factor in determining the long-term effects of these collisions. Young inflated planets will be

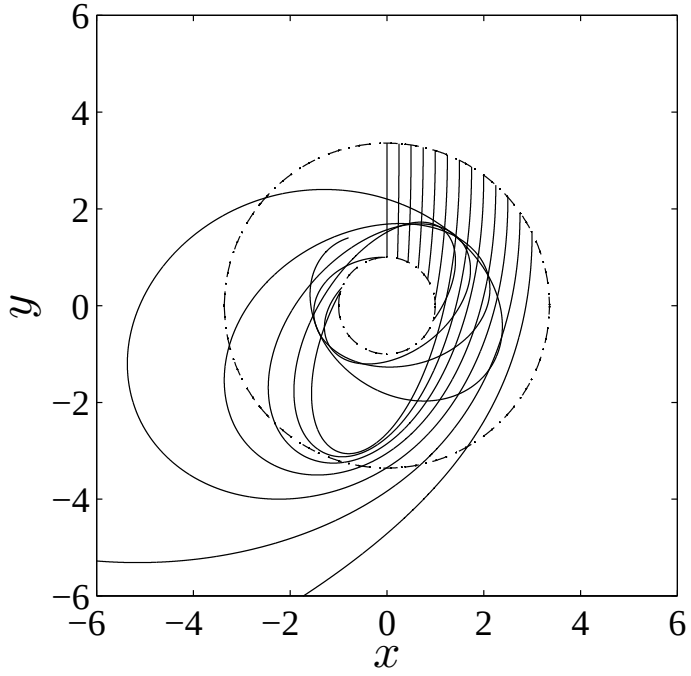

Fig. 12.— Trajectories with constant initial velocity $v_0 = 50$ km s^{-1} and varying impact parameters. The outer dashed circle marks the location of the surface of the Jovian planet; the inner dashed circle indicates the core radius, which has dimensionless radius $\xi_c = 1$. The Jovian planet has mass $M_P = 1 M_J$, but an inflated radius $R_P = 2 R_J$. With this inflated radius, the capture cross section is slightly reduced, and rocky planets are able to penetrate the gaseous envelope more easily. Nonetheless, nearly all incident planets remain gravitationally bound.

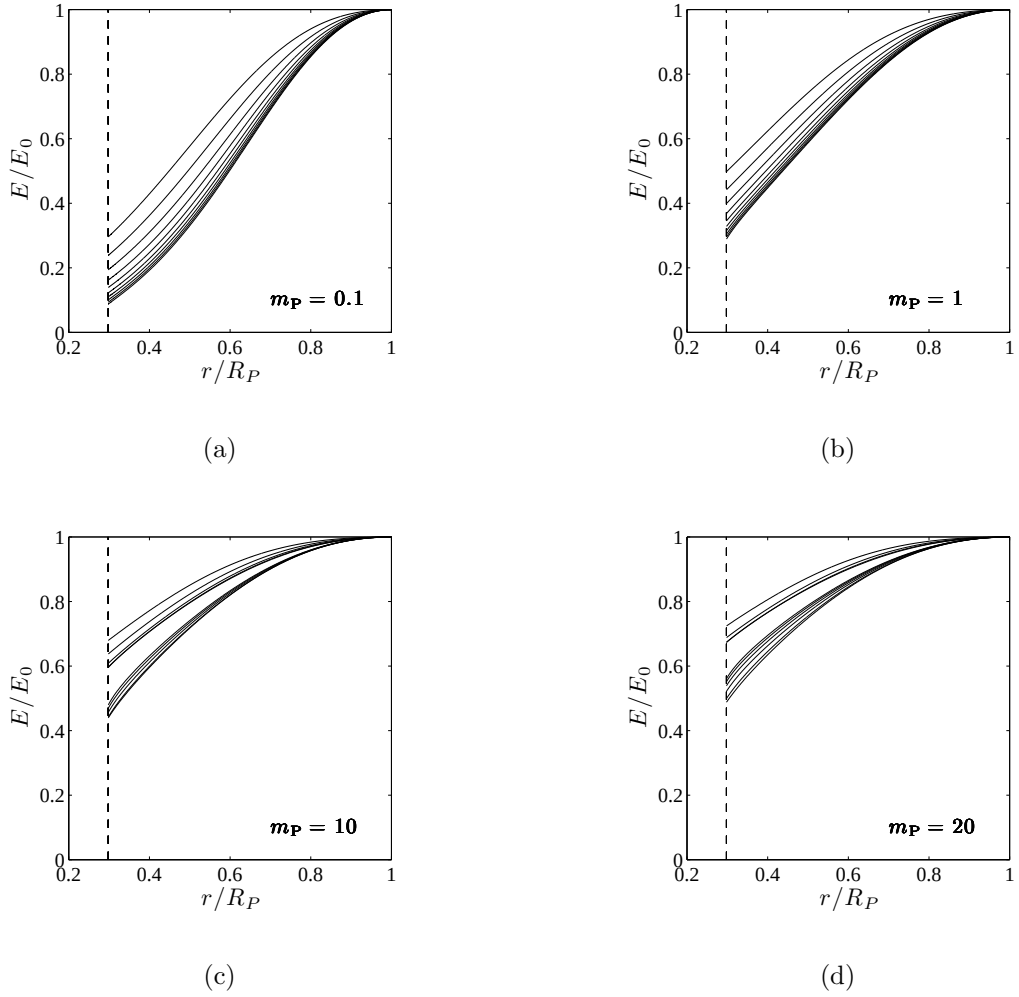

Fig. 13.— Same as Figure 9, but with an inflated Jovian planet radius $R_P = 2R_J$, typical of a young gaseous planet. Such planets are much less efficient at dissipating the kinetic energy of the rocky planet, and the fraction remaining when the projectile strikes the core can be as high as $E_f/E_0 \approx 0.75$

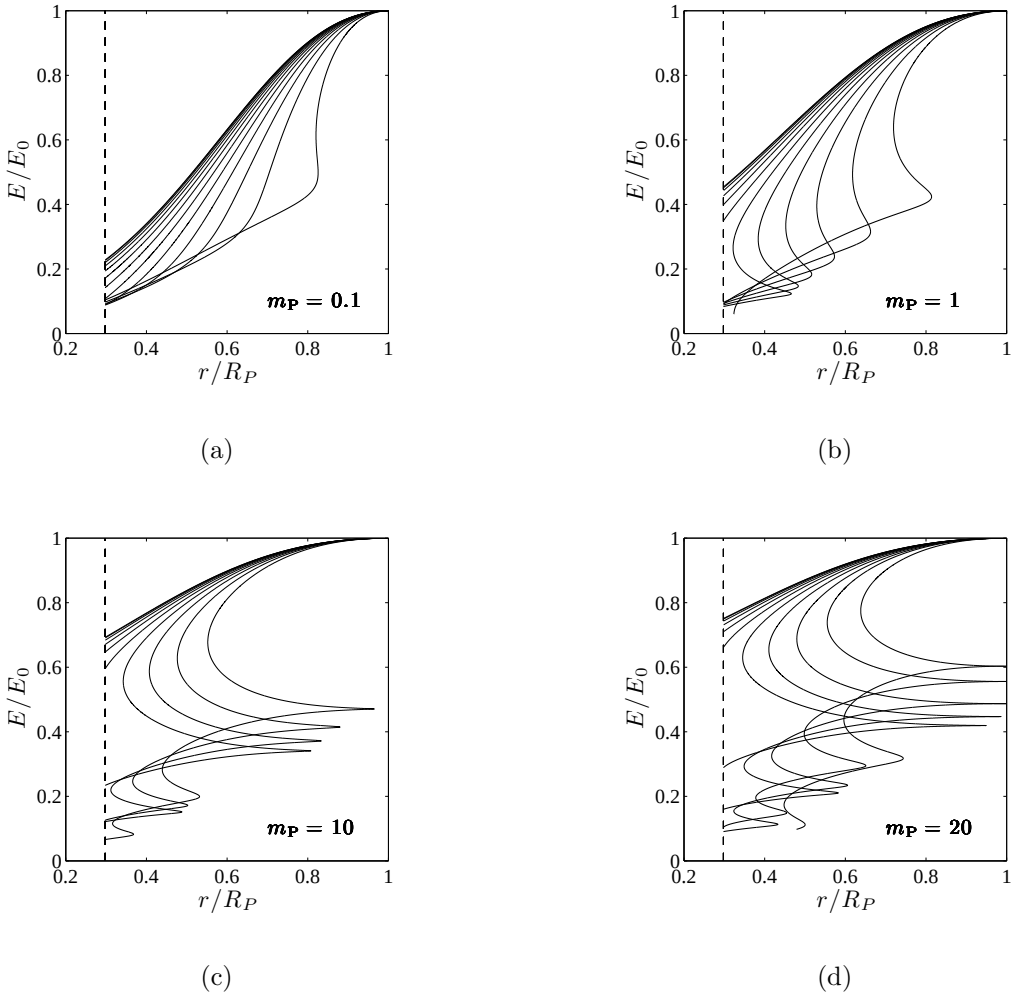

(a) (b)

(c) (d)

Fig. 14.— Same as Figure 10, but with a Jovian planet radius $R_P = 2R_J$, typical of a young gaseous planet. The energy fraction E/E_0 remains relatively high for small impact parameters, but decreases drastically beyond a critical value $x_* \approx \xi_c$. The rocky planet orbits can have many turning points in this scenario, which allows the energy fraction to take on multiple values for the same radius.

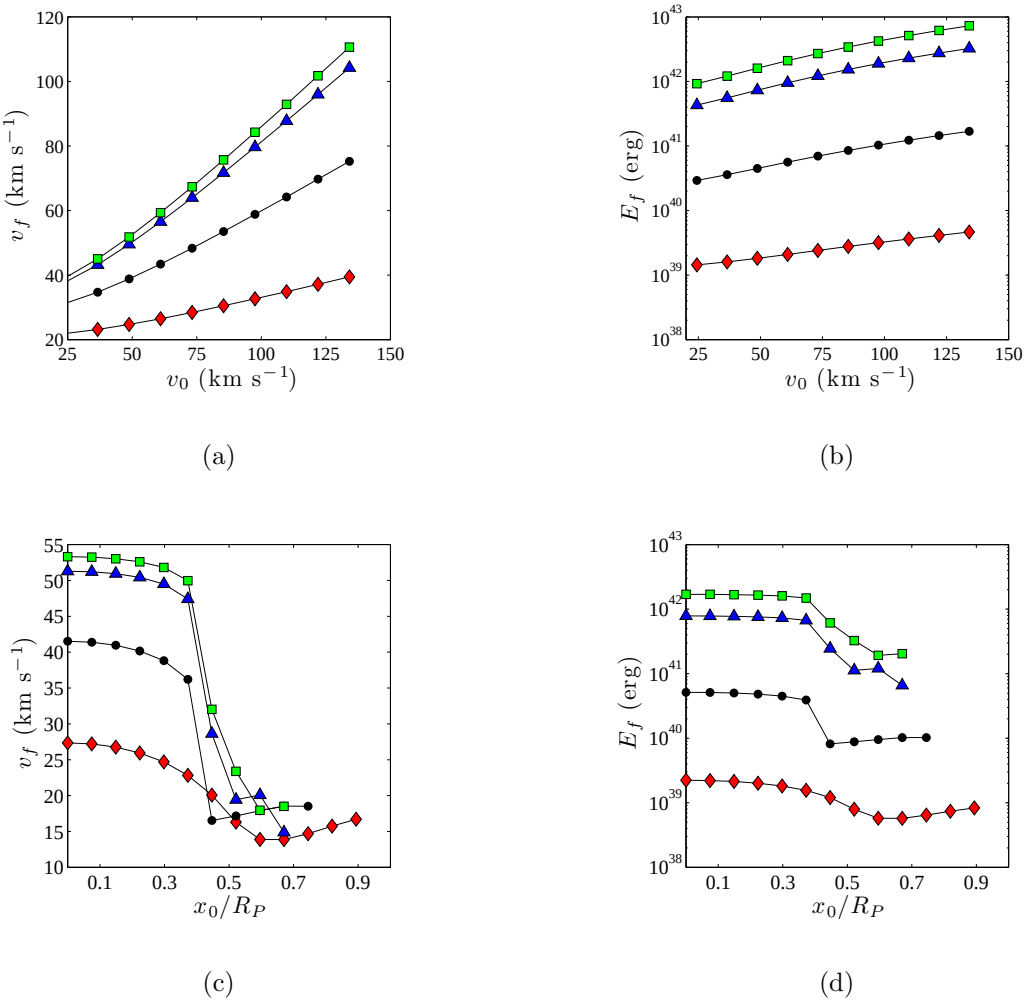

Fig. 15.— Same as Figure 11, but with a Jovian planet radius $R_P = 2R_J$. Since there is less frictional dissipation, the kinetic energy of the larger planets can actually increase as they fall into the potential well of the Jovian planet. With radius $R_P = 2R_J$, the kinetic energy deposited to the core is larger than $R_P = 1R_J$ by nearly an order of magnitude.

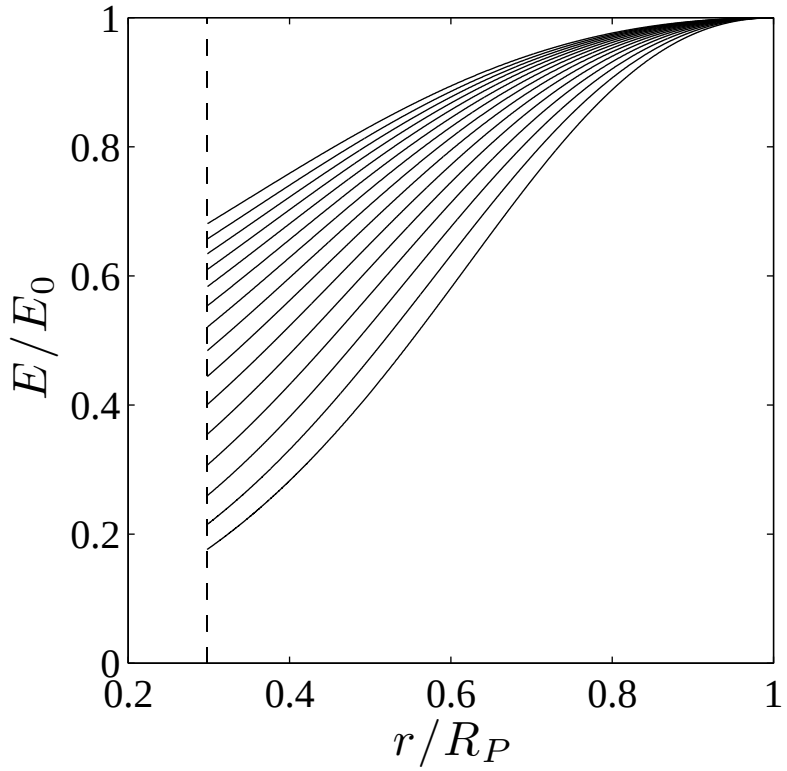

Fig. 16.— Energy fraction E/E_0 for various Jovian planet radii. Each curve corresponds to a trajectory within a Jovian planet of mass $M_P = 1M_J$ and radius $R_P = 0.7R_J$ (bottom) to $R_P = 2.1R_J$ (top). The rocky planet has mass $m_{\rm p} = 10M_\oplus$, initial velocity $v_0 = 50$ km s^{-1}, and impact parameter $x_0 = 0$ (head-on collision). Dashed line indicates the core radius ξ_c. The fraction of kinetic energy dissipated along the trajectory increases drastically with decreasing Jovian planet radius.

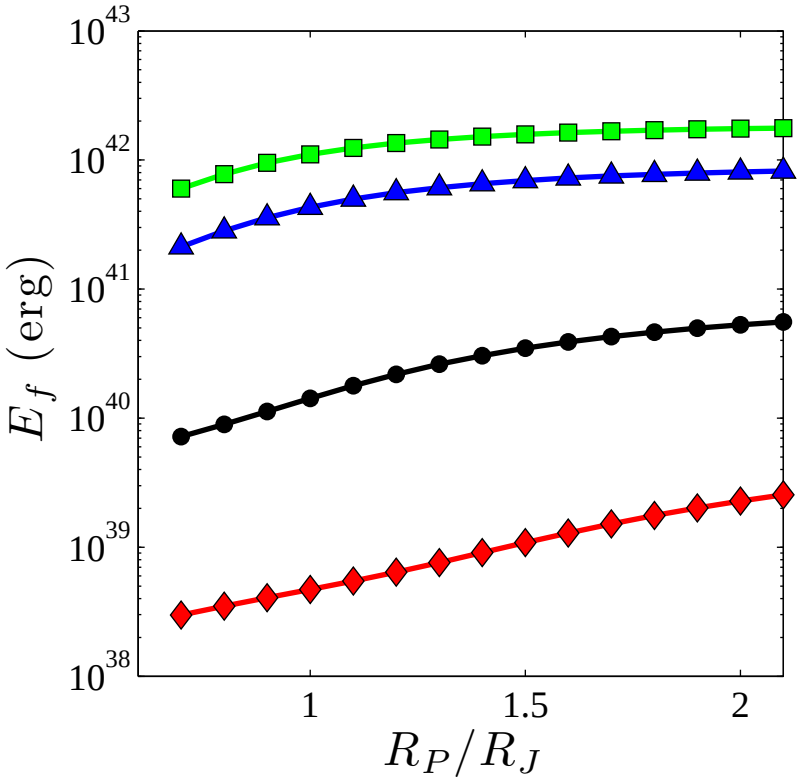

Fig. 17.— Effects of the Jovian planet radius on the kinetic energy dissipation. The four curves correspond to rocky planet masses $m_{\rm p} = 0.1, 1, 10$ and $20 M_\oplus$ (from bottom to top), each with initial velocity $v_0 = 50$ km s^{-1} and impact parameter $x_0 = 0$. The Jovian planet has mass $M_P = 1 M_J$, polytropic index $n = 1$, and core radius $\xi_c = 1$. The amount of kinetic energy delivered to the core is much higher for the radii at the upper end of this range.

more susceptible to prolonged heating than mature planets. Similarly, close-in exoplanets (Hot Jupiters) will be more susceptible than giant planets farther from their host stars.

To conclude the discussion on energy dissipation, we present the following analytic estimate for the kinetic energy T_f remaining when a rocky planet reaches the core. For the particular case of direct collisions, with impact parameter $x_0 = 0$, incoming planets will travel along a radial path from the giant planet surface to the core. The amount of energy dissipated along this path is given by

$$W = \alpha \int_{\xi_c}^{\xi_0} f^n v^2 \, d\xi, \tag{34}$$

where the signs have been chosen so that $W > 0$, and where all quantities are dimensionless. Using equation (30) to estimate the speed as a function of position, the work W can be expressed as

$$W = \alpha {v_0}^2 \int_{\xi_c}^{\xi_0} f^n e^{2\beta(\xi - \xi_0)} \, d\xi, \tag{35}$$

where $\beta = \alpha \langle f^n \rangle$. If we make the approximation $\langle f^n \rangle \approx 1/2$, the expression becomes

$$W = \frac{1}{2} \alpha {v_0}^2 \int_{\xi_c}^{\xi_0} e^{\alpha(\xi - \xi_0)} \, d\xi, \tag{36}$$

which can be integrated to yield

$$W = \frac{1}{2} {v_0}^2 [1 - e^{\alpha(\xi_c - \xi_0)}] = T_0 [1 - e^{\alpha(\xi_c - \xi_0)}]. \tag{37}$$

Conservation of energy implies $T_f = T_0 - W$, where T_0 and T_f are the initial and final kinetic energies, so the remaining energy when these planets reach the core is given by

$$T_f = e^{\alpha(\xi_c - \xi_0)} T_0. \tag{38}$$

For a giant planet with polytropic index $n = 1$ and core radius $\xi_c = 1$, the final predicted energies for rocky planets with masses $m_{\rm p} = 1, 10$, and $20 M_\oplus$ are given by $T_f/T_0 \sim 0.03$, 0.20, and 0.30, in rough agreement with the numerical results. Due to the approximations introduced, equation (38) works best for small values of the friction coefficient, and worsens as α increases.

4. Tidal Disruption

For the purposes of calculating their orbits, the impinging planets have thus far been treated as indestructible point particles. In this section, we consider the possibility that

these planets can be disrupted by tidal forces. If the planet is destroyed, several outcomes are possible. Depending on the interior conditions of the giant planet, the rocky planet remnants could either become accreted onto the core, or uniformly enrich the envelope with heavy elements. A full determination of the outcome is beyond the scope of this present work; in addition, it requires a better understanding of gas planet interiors (e.g., including convection) than is currently available. In this section we consider how tidal forces act on the incoming rocky planets and determine the likelihood of these bodies reaching the core (of the Jovian planet) relatively intact. These results allow us to specify the maximum amount of energy and mass deposited at the planetary core.

At any point in the trajectory, the tidal force (per unit mass) exerted on the rocky planet can be approximated by the difference in the gravitational acceleration at the near and far surfaces,

$$\Delta F = \frac{GM(r)}{r^2} - \frac{GM(r+\Delta r)}{(r+\Delta r)^2}, \tag{39}$$

where $\Delta r = 2r_{\rm p}$ (the rocky planet diameter). Note that the tidal forces arise due to the small difference in the enclosed mass as well as the difference in radial distance. Since the tidal forces are not spherically symmetric with respect to the rocky planet, this treatment introduces an approximation. Nonetheless, if the orbiting planet is to withstand these tidal forces, the tidal acceleration given by equation (39) must be less than the surface gravity of the rocky planet. Equating these quantities yields the condition for survival, i.e.,

$$\left| \frac{GM(r)}{r^2} - \frac{GM(r+\Delta r)}{(r+\Delta r)^2} \right| = \frac{Gm_{\rm p}}{{r_{\rm p}}^2}. \tag{40}$$

This expression can be simplified by making the following expansions

$$M(r+\Delta r) \approx M(r) + \frac{dM}{dr}\Delta r, \tag{41}$$

and

$$\frac{1}{(r+\Delta r)^2} = \frac{1}{r^2}\left(\frac{1}{(1+\Delta r/r)^2}\right) \approx \frac{1}{r^2}\left(1 - \frac{2\Delta r}{r}\right). \tag{42}$$

Neglecting all terms higher than first order in $\Delta r/r$, the expression for the tidal force takes the form

$$\Delta F = \frac{4r_{\rm p}GM(r)}{r^3} - 8\pi r_{\rm p} G\rho(r). \tag{43}$$

Near the surface of the Jovian planet, the density is small enough so that the second term on the right hand side can be neglected. After dividing by $r_{\rm p}$ we obtain a rough criterion for the survival of the rocky planet,

$$\frac{4M(r)}{r^3} \leq \frac{m_{\rm p}}{{r_{\rm p}}^3}. \tag{44}$$

In other words, the orbiting body will be tidally disrupted if its mean density is less than about four times the mean density of the giant planet (considering the enclosed mass only). Note that equation (44) is only approximately valid at the surface of the Jovian planet, where the differential change in the enclosed mass and the ratio $(\Delta r)/r$ are relatively small. Here we are considering rocky planets with radii $r_{\rm p} \sim 1R_\oplus$, and giant planets with radii $R_P \sim 10R_\oplus$, so that the ratio $(\Delta r)/r \sim 0.2$ at the surface and increases with decreasing radial position. As a result, the approximation scheme deteriorates rapidly as the rocky planet moves inward. In spite of these approximations however, equation (44) provides a simple, order of magnitude estimation of the tidal stretching at the giant planet surface.

Notice that the two sides of equation (44) are nearly equal for a pair of planets with the mean density of Jupiter and Earth (where $\langle\rho\rangle \sim 1.3$ g cm^{-3} and ~ 5.5 g cm^{-3} respectively). As a result, an Earth-like planet can be tidally disrupted by a giant planet like our Jupiter, but very well may survive if the radius of the Jovian planet is somewhat larger (so that its density is lower). This shows that these planets will experience significant tidal forces and could deform considerably; however, more accurate calculations are needed to determine the extent of this tidal deformation.

The ratio of the tidal force to the surface gravity of the rocky planet as a function of radial distance can be accurately calculated from equation (40). Here we explore a variety of planetary properties. The Jovian planet mass was held constant at $M_P = 1M_J$ and the radius was varied from $R_P = 1 - 2\ R_J$ leading to average densities of order $\langle\rho\rangle = 0.1 - 1.0$ g cm^{-3}. The results are shown in Figures 18 through 20 for Jovian planet radii $R_P = 1R_J$ (top panels) and $R_P = 1.2R_J$ (bottom panels), where the latter values are appropriate for inflated Hot Jupiters (Laughlin et al. 2011), and for rocky planet masses $m_{\rm p} = 0.1, 1$ and $10M_\oplus$. Each curve represents a different rocky planet density, in the range 2 - 10 g cm^{-3} (Valencia et al. 2007). All results shown are for coreless polytropes of index $n = 1$; adding a core does not significantly affect the strength of the tidal forces (and hence the curves in these diagrams), so these results can be generalized to include structures with cores.

Notice that the tidal force ΔF vanishes at radii $r \sim R_P/2$. This force becomes negative for smaller radii, indicating that an orbiting planet will first be stretched and subsequently compressed during its inward trajectory. In the center of the Jovian planet (where $r \to 0$), the compression reaches a maximum and the force given by equation (40) formally approaches a well-defined limit

$$\lim_{r\to 0} \Delta F = -\frac{8\pi}{3} G\rho_c r_{\rm p}. \tag{45}$$

Not that this is a (mathematically) formal result, because we are taking the limit $r \to 0$ but the rocky planet has finite radius.

The area between the dashed lines (set where $\Delta F/f_{\rm p} = \pm 1$) in Figures 18 through 20 indicates the regions where the surface gravity of the rocky planet can withstand the tidal acceleration. If the ratio $\Delta F/f_{\rm p} > 1$ the outermost layers of the planet are stripped away; if $\Delta F/f_{\rm p} < -1$ the planet experiences devastating levels of compression. Here we consider a rocky planet to survive whenever the condition $|\Delta F/f_{\rm p}| < 1$ is satisfied all the way to the core. In general, all but the very smallest planets are able to penetrate deep into the interior (at least 50 - 70% of the distance to the center) before experiencing severe tidal disruption; in many cases, the rocky planets reach the core intact. As expected, the small planets ($m_{\rm p} \sim 0.1 M_{\oplus}$) must be very dense to survive the entire trajectory, and we exclude them in the remaining analysis. For Jovian planets with average densities of Jupiter (1.3 g cm^{-3}), the mean rocky planet density must be greater than $\rho_{\rm p} \approx 5-6$ g cm^{-3} for $m_{\rm p} = 1 M_{\oplus}$; larger rocky planets with $m_{\rm p} = 10 M_{\oplus}$ can survive with somewhat lower density $\rho_{\rm p} \approx 3-4$ g cm^{-3}. For Jovian planets with radius $R_P = 2 R_J$, the rocky planets easily avoid tidal disruption (not shown). On the other hand, for Jovian planets with high densities (roughly where the inequality of equation [44] is violated), the tidal forces at the gaseous surface can exceed the rocky planet surface gravity, and such planets are tidally disrupted before even entering the atmosphere.

After a rocky planet is tidally disrupted, its fate remains unclear, and should be the subject of further study. The resulting rocky debris could continue the journey toward the core, thereby increasing the final core mass of the Jovian planet. Alternatively, the debris could remain in the envelope and uniformly enrich the atmosphere. The outcome will depend on, among other things, the opacity of the Jovian planet. High opacities could lead to convection, which causes the planet remnants to be uniformly mixed into the gaseous planetary interior.

In summary, we find that large rocky planets ($m_{\rm p} \gtrsim 10 M_{\oplus}$) have a good chance of reaching the core intact, and even planets with $m_{\rm p} \sim 1 M_{\oplus}$ are able to survive in many cases, as long as the Jovian planet density is sufficiently low. As a result, these collisions provide a viable mechanism for increasing the cores of gaseous giant planets, especially those with inflated radii like young Jovian planets, as well as much of the observed Hot Jupiter sample.

5. Conclusion

This thesis explores collisions between Jovian planets and smaller terrestrial bodies in order to identify possible changes in the structure of the larger planet. This work focuses on the scenario where the Jovian planet has migrated inward and entered into a tight orbit around its star, and subsequently experiences collisions with rocky planets that migrate later.

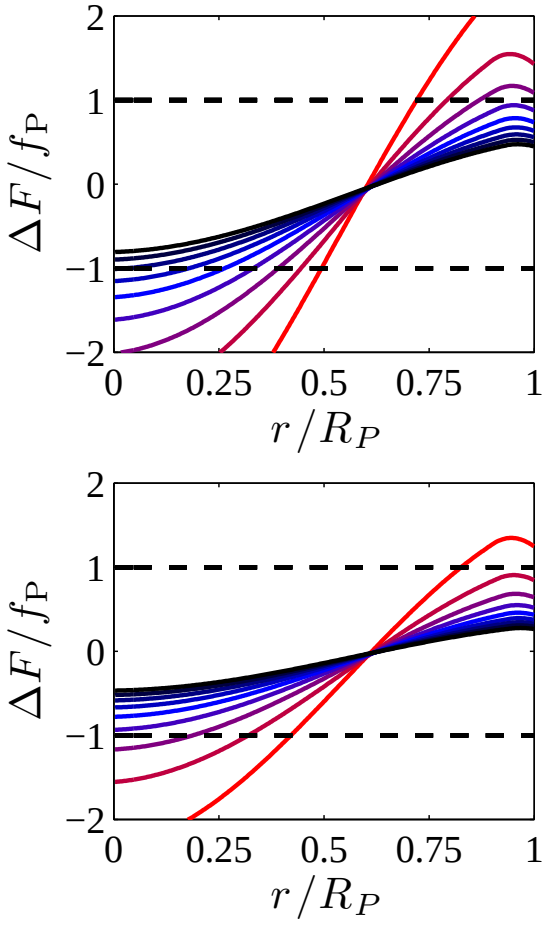

Fig. 18.— Ratio of tidal forces to surface gravity as a function of radial distance for rocky planets of mass $m_{\rm p} = 0.1 M_{\oplus}$. Coreless Jovian planet with fixed mass $M_P = 1 M_J$ and radius $R_P = 1 R_J$ (top panel), and $R_P = 1.2 R_J$ (bottom panel), where the latter is appropriate for an inflated Hot Jupiter. Each curve corresponds to a rocky planet with a different mean density, ranging from 2 (top red), to 10 (bottom black) g cm^{-3}. The region between the dashed lines indicates points where the rocky planet can survive. For the inflated Jovian planet, only the projectile with the lowest density is tidally disrupted at the surface.

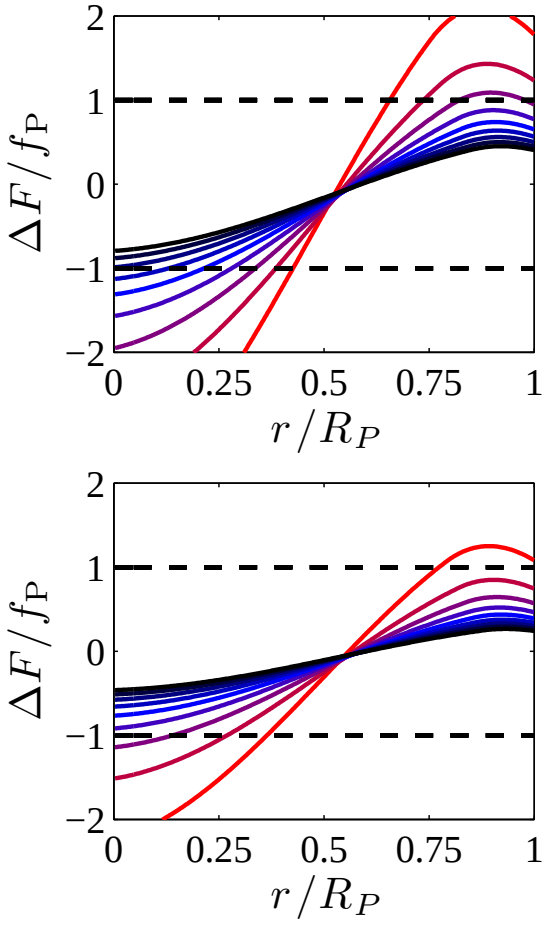

Fig. 19.— Ratio of tidal forces to surface gravity as a function of radial distance for rocky planets of mass $m_{\rm p} = 1M_{\oplus}$. Coreless Jovian planet with mass $M_P = 1M_J$ and radius $R_P = 1R_J$ (top panel), and $R_P = 1.2R_J$ (bottom panel), where the latter is appropriate for an inflated Hot Jupiter. Each curve corresponds to a rocky planet with a different mean density, ranging from 2 (top red), to 10 (bottom black) g cm^{-3}. The region between the dashed lines indicates points where the rocky planet can survive. For the inflated Jovian planet, only the projectile with the lowest density is tidally disrupted at the surface.

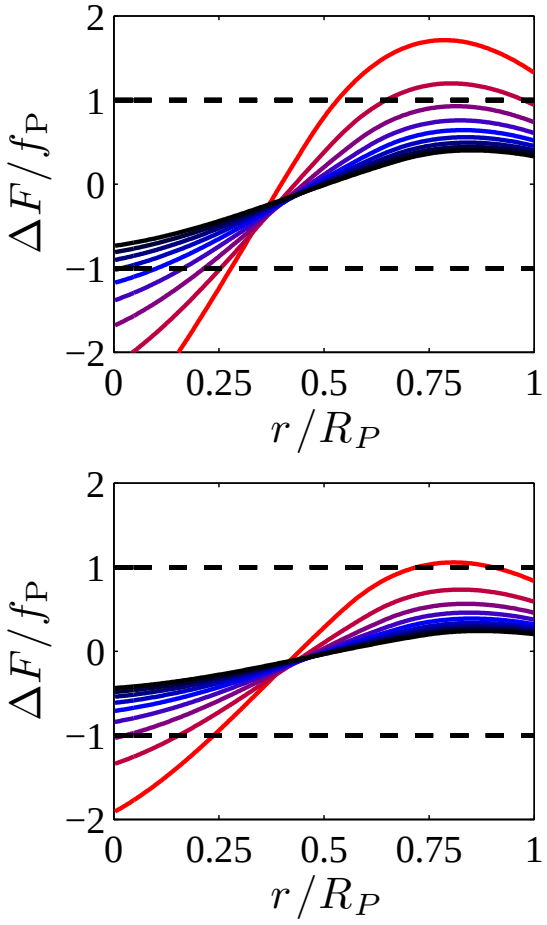

Fig. 20.— Ratio of tidal forces to surface gravity as a function of radial distance for rocky planets of mass $m_{\rm p} = 10 M_\oplus$. Coreless Jovian planet with mass $M_P = 1 M_J$ and radius $R_P = 1 R_J$ (top panel), and $R_P = 1.2 R_J$ (bottom panel), where the latter is appropriate for an inflated Hot Jupiter. Each curve corresponds to a rocky planet with a different mean density, ranging from 2 (top red), to 10 (bottom black) g cm^{-3}. The region between the dashed lines indicates points where the rocky planet can survive. Rocky planets with larger masses, as in this plot, are able to withstand the tidal forces much more easily.

However, many of the results apply to other parts of the parameter space, e.g., the possible accretion of cores by gaseous planets formed via gravitational instability (e.g., Boss 1997; Boley 2009). These collisions can affect the structure of the target giant planets in three ways: [a] The metallicity is increased, [b] the core size can be increased, and [c] a substantial amount of energy is imparted to the giant planet. For Hot Jupiters, these impacts could thus help explain the observed anomalous radius distribution, in terms of both long-term heating and the accumulation of heavy elements.

Rocky planets are efficiently captured by giant planets and thereby increase the metallicity of the larger body. For sufficiently high impact speeds v_0 and/or large impact parameters x_0, the projectile planet can pass through the giant planet and emerge out the other side. For nearly head-on collisions, the initial speed required to avoid permanent capture is much higher $v_{\rm pen} > 10^4$ km s^{-1} than the expected impact speeds $v_0 \approx 40 - 150$ km s^{-1}. With these latter speeds, incoming planets can escape only for impact parameters comparable to the radius of the Jovian planet, where the density is low. In other words, permanent capture is avoided only when the rocky planet skims the surface of the Jovian target. As a result, most rocky planets lose enough kinetic energy through their initial passage that they remain gravitationally bound and are captured. Nonetheless, the capture cross section of the target planet can be reduced in some cases; for collision speeds $v_0 \gtrsim 100$ km s^{-1}, the cross section is smaller than the geometric area by $\sim 30\%$ (see Figure 7).

These conditions provide a plausible mechanism for explaining the massive cores that have been inferred for the observed Hot Jupiters, e.g., the planet HD 149026b (Sato et al. 2005). Although metallicity increases are essentially automatic through such collisions, core masses can probably only increase if the rocky planets avoid tidal disruption and survive to reach the central regions. The parameter space includes cases where the impinging planets survive, as well as cases where they are destroyed by tidal forces. Rocky planets with the mass and radius of Earth, when they encounter Jovian planets having the mass and radius of Jupiter, live near the threshold for tidal destruction. However, when such planets encounter Jovian-mass planets with inflated radii $R_P \gtrsim 1.2 R_J$, most are able to survive all the way to the central regions. This finding is relevant because Hot Jupiters are subjected to additional heating sources and are thus larger in radius for a given mass. Furthermore, such collisions are expected to occur early in the system's evolution when the giant gaseous planets are even larger.

For collisions to significantly alter the metallicity or the core mass of a giant planet, the planet must accrete rocky bodies of total mass $\Delta M \sim 10 - 100 M_\oplus$. The accumulation of such mass increments could take place through collisions with many smaller rocky bodies or via fewer larger bodies. Large rocky bodies, with mass $m_{\rm p} > 10 M_\oplus$, are more effective

for several reasons. First, larger bodies are subjected to less eccentricity damping during migration, and are thus more likely to collide with the giant planets. More specifically, eccentricity damping will be small enough to allow collisions when the rocky planets are large enough to partially clear gaps in the disk (Artymowicz 1993; Kley et al. 2004), which occurs when their Hill sphere exceeds the disk scale height (Crida et al. 2008; Papaloizou & Terquem 2006). These considerations indicate that relatively large rocky planets (with mass $m_{\rm p} \approx 10 - 20 M_\oplus$) are favored in order to achieve partial gap-clearing, reduced eccentricity damping, and ultimately collisions. In addition, collisions with larger rocky bodies allow for the necessary mass increments to be realized through a lower number of encounters. Finally, as we have shown, larger rocky bodies are more likely to survive tidal disruption and reach the central regions. This has helped constrain the planet masses that should be used in future theoretical work. On the other hand, if the circumstellar disk has high levels of turbulence, small rocky planets are subject to stochastic migration (e.g., Adams & Bloch 2009) and can still experience encounters with giant planets. Such encounters often result in collisions (Ketchum et al. 2011b) when they take place at small semi-major axes ($a \lesssim 0.1$ AU); for larger $a \gtrsim 1$ AU, most encounters result in ejection of the smaller planet, with collisions taking place only $\sim 10\%$ of the time (Ketchum et al. 2011a)

Collisions can provide a substantial amount of energy to the target giant planet. For rocky planets with mass $m_{\rm p} = 10 M_\oplus$ and initial speed $v_0 = 60$ km s^{-1}, the kinetic energy transferred to the giant planet is $\Delta E \sim 10^{42}$ erg. If, for example, this energy is radiated over a time scale of 1 Gyr, the associated increment in the planetary luminosity would be $\Delta L_P \approx 4 \times 10^{18}$ W, which could be large enough to affect the internal structure of the planet (Bodenheimer et al. 2003). However, in order to provide the gaseous planet with a long-term energy source, most of the energy must be deposited deep in the interior, in regions of high opacity. For a given rocky planet mass, the amount of energy deposited depends on the density of the Jovian planet. For a Jovian planet with the mass and radius of Jupiter, most of the kinetic energy is deposited in the outer planetary layers. At the other end of the possible range, for a Jovian planet with the mass of Jupiter and an inflated radius $R_P = 2 R_J$, little energy is deposited in the outer layers and a sizeable fraction is delivered to the core.

An important unresolved issue is the question of how quickly the collision-induced energy is transferred out of the planet. Collisions with large terrestrial planets deposit enough kinetic energy in the central regions to potentially affect the structure, and could even play a role in explaining the radius anomalies of the inflated exoplanets if the time scales for energy loss are sufficiently long. In future work, interior models of Hot Jupiters should be modified to include this possible energy source.

As shown herein, incoming rocky bodies are sometimes tidally destroyed after entering

the surface of the giant planet (see also Anic et al. (2007) and Li et al. (2010) for detailed simulations of specific cases). This work indicates that most planets heavier than $m_{\rm p} \sim 10 M_\oplus$ are able to withstand tidal disruption; however, these planets can also experience devastating levels of ablation. Through both ablation and tides, incoming planets continuously lose mass throughout their descent, and these effects should be studied in future work. Ablation will thus increase the overall metallicity of the Jovian planet atmosphere and reduce the amount of mass (and kinetic energy) delivered to the core. More detailed knowledge of these ablation effects is especially important for the development of energy transport models, because any increases in metallicity in the outer layers will affect the transport of heat. If ablation is strong enough, the rocky planets could completely disintegrate before reaching the core, even if they avoid being tidally disrupted. Since the calculations of this paper do not include ablation effects, the quantities of heat and heavy elements deposited in the deep regions of the Jovian planet will be lower than estimated herein. This thesis thus provides an upper limit on these quantities.

The results of this paper show that the mean density of the giant planet plays an important role in determining the consequences of these collisions. The average density helps determine whether or not incoming rocky planets can survive tidal disruption, as well as the radial layers where most of the kinetic energy is deposited. Since giant planets are born with large radii, this density dependence translates into a dependence on the age of the planet. A rocky planet that collides with a young giant planet (with low density) can have dramatically different consequences than a rocky planet that collides with a mature giant planet (with high density). The environment in which the giant planet resides plays an additional role. Since Hot Jupiters often remain significantly inflated throughout their evolution, this subset of extrasolar planets should be even more sensitive to these collisions. This lend promising support for the proposal that planetary impacts could help explain, in part, the anomalous radius distribution of the observed Hot Jupiters.

Acknowledgments

I would like to thank my advisor Fred Adams for supervising this project, and for being an incredible mentor. Under his guidance, I have developed my research skills, and have learned a great deal about about physics, astronomy, and mathematics. I look forward to further collaboration.

This research was supported by a grant from the University of Michigan Honors Summer Fellows program.

Portions of this thesis have been submitted to Publications of the Astronomical Society of the Pacific (PASP) as Anderson & Adams 2012; this paper is currently under review.

A. Estimate of the Collision Frequency

In this Appendix we present a simple estimation of the collision frequency for Jovian planets at varying locations in the circumstellar disk, following a formulation similar to that of Helled & Schubert (2009) to determine planetesimal accretion rates for Jovian protoplanets. The collision frequency, denoted by Γ, takes the form

$$\Gamma = n_{\oplus} \sigma v, \tag{A1}$$

where $n_{\oplus}$ is the number density of rocky (projectile) planets, σ is the cross section of the Jovian (target) planet, and v is the relative velocity between the two bodies. The number density of rocky planets is a function of both radial location in the disk and time; however, we neglect the time dependence here. As a simple approximation, $n_{\oplus}$ is given by $n_{\oplus} = \Sigma_R / 2H$, where $\Sigma_R(r)$ is the surface density of rocky material in the disk, and $H(r)$ is the scale height. Specification of both of these quantities requires some assumptions on the properties of the disk. Following the general approach of this paper, we adopt simple forms for both Σ_R and H:

$$\Sigma_R = \Sigma_0 \left(\frac{R_d}{r} \right)^{3/2}, \tag{A2}$$

and

$$H = \frac{a_s}{\Omega}, \tag{A3}$$

where Σ_0 is the surface density at the edge of the disk, R_d is the radius of the disk, a_s is the sound speed, and $\Omega^2 = GM_*/r^3$, the Keplerian frequency. Note that a_s depends on the temperature ($a_s \sim T^{1/2}$), and hence location in the disk, and we adopt a power-law temperature profile, of the form

$$T = T_0 \left(\frac{R_*}{r} \right)^q, \tag{A4}$$

where q lies in the range $1/2 - 3/4$, and we set $T_0 = 5000$ K (the surface temperature of a solar-type star) for this calculation. If we assume that the rocky material is divided into planets of equal mass $m_{\rm p} = 1 M_{\oplus}$, the total number of rocky planets in the disk can be estimated by integrating Σ_R over the entire area of the disk:

$$N_{\oplus} = \int_{R_*}^{R_d} 2\pi r \Sigma_0 \left(\frac{r}{R_d} \right)^{-3/2} dr, \tag{A5}$$

which evaluates to

$$N_\oplus = 4\pi {R_d}^2 \Sigma_0. \tag{A6}$$

The mass of heavy elements in the disk is related to the total mass of the disk by $M_R = zM_d$, where z can take a range of values. Typical disk parameters are $z = 1/100$ and $M_d = M_*/10$. Assuming $M_* = 1M_\odot$, the total number of earth-mass planets is $N_\oplus = zM_*/10M_\oplus \approx 300$. Thus, $\Sigma_0 = 300/4\pi {R_d}^2$. Substituting these relations into equation (A1) produces

$$\Gamma = \frac{N_\oplus v {R_P}^2}{8H {R_d}^2} \left(\frac{r}{R_d}\right)^{-3/2}, \tag{A7}$$

where we have assumed a minimum (geometric) cross section $\sigma = \pi {R_P}^2$, but the actual value of σ is related to the gravitational capture cross section, and depending on the energy of the projectile planet, can be somewhat larger. Thus, by specifying the relative velocity between the target and projectile planets and the radius of the disk, the collision frequency is determined. Here we adopt disk radius $R_d = 100$ AU. For a Jovian planet with a semi-major axis 1 AU, and a relative velocity of 10 km s^{-1} between the projectile rocky planet and target Jovian planet, the collision frequency predicted by equation (A7) is $\Gamma \approx 25$ Myr^{-1}, and even higher for giant planets located at small semi-major axes. We note that this calculation does not account for the fact that the collision frequency is a decreasing function of time. As a result, this value of Γ cannot be maintained, and the average value over the time intervals of interest here ($\sim 3 - 10$ Myr) will be lower. Nonetheless, we have shown that the expected frequency of collisions can be significant for typical values of the disk parameters. Even if we suppose that the actual (average) collision frequency is much lower, say $\Gamma \sim 2$ Myr^{-1}, over a period of 5 Myr, a gaseous giant planet could still accrete as many as 10 rocky planets.

B. Asymptotic Dynamical Behavior

This Appendix explores the dynamics of a test particle in a coreless polytropic potential in the limit of small radial coordinate ξ. Although this study has no immediate physical applications, it presents an interesting dynamical problem. Motivated by the seemingly continuous inward spirals of the test particles shown in Figure 5, we attempt to determine whether the particles will eventually come to rest at the origin, or approach the origin asymptotically.

For simplicity, we examine purely radial motion, where the test particle has zero angular momentum (impact parameter $x_0 = 0$). In this scenario, the particle oscillates about the origin in a straight line, and as time increases, the amplitude of the oscillations decreases. This motion is nicely depicted in the two dimensional phase space $(\xi, \dot{\xi})$ as motion in a spiral

around the origin in Figure 21. Although this plot clearly indicates that the amplitude of the oscillations decreases with time, it is unclear whether the particle will eventually come to rest at the origin (in a finite amount of time), or oscillate about the origin indefinitely (with an asymptotically decreasing amplitude). To help address this issue, integrations have been carried out to large times and the resulting motion analyzed in terms of the quantity $\mathcal{R} = \left(\xi^2 + \dot{\xi}^2\right)^{1/2}$. This quantity has the characteristics of an energy function. If the test particle comes to rest in a finite amount of time, $\mathcal{R}$ should reach zero in a finite amount of time. In Figure 22 is a plot of $\mathcal{R}(\tau)$, where τ is the dimensionless time variable defined in equation (10). After the initial inward trajectory, the particle settles into near periodic motion, with $\mathcal{R}$ just slightly reduced after each cycle. The plot shows that $\mathcal{R}$ continues to decrease indefinitely, which indicates (but does not prove) that the particle will oscillate forever. However, note that the integrations have been performed to very long time intervals ($\tau \approx 10^4$). For comparison, the typical time scale for the particle to travel the initial passage from the polytrope surface to the center is $\tau \approx 10$, or $t = t_0\tau \approx 1$ hr. It is therefore unlikely that the behavior will differ in the limit $\tau \to \infty$. From Figure 22, the slope of $\mathcal{R}$ approaches a constant value, indicating a power-law relation for $\mathcal{R}(\tau)$:

$$\mathcal{R} \sim \tau^{-a}, \tag{B1}$$

where $a \approx 1$. Thus, we conclude that the particle will come to rest at the origin only as $\tau \to \infty$.

C. Tidal Disruption of Rocky Planets Near White Dwarfs

Accretion events are common in planetary systems, and many of the results of this thesis can be applied to other situations. For example, there is observational evidence for the accretion of terrestrial planets onto white dwarfs (e.g., Jura 2003; Vennes et al. 2010), due to enrichments of heavy elements (calcium, magnesium, silicon, and other metals) in the stellar atmospheres. Since white dwarfs are composed mostly of carbon and oxygen, it is difficult to explain this enrichment of heavy elements without the accretion of some secondary rocky planet or asteroid. The reasons are as follows. White dwarfs arise from intermediate mass stars, with $M_* \lesssim 8M_\odot$. After leaving the main-sequence with a helium core surrounded by a hydrogen envelope, such stars attain the central core temperature necessary for helium ignition ($T_c \approx 10^8$ K), and begin a (brief) period of sustained helium fusion. Eventually a core of carbon and oxygen accumulates, but cannot be further ignited, because the effects of degeneracy pressure stabilize the star before the necessary central temperatures are reached. Such stars thus end their lives as white dwarfs composed of carbon and oxygen, with thin outer shells of hydrogen and/or helium (see, e.g., Prialnik 2010), and heavier elements should

only occur in trace amounts. This indicates that the observed stars with heavier elements have accreted additional material, perhaps in the form of smaller rocky planets and asteroids.

As a further application of the tidal force analysis derived herein, we apply the methods of Section 4 to this scenario, and compute the radius surrounding the white dwarf where terrestrial bodies will be tidally disrupted. The polytropic index is fixed at $n = 1.5$, which is appropriate for degenerate stars (Chandrasekhar 1939; Phillips 1994). The Jovian planet mass M_P is replaced with white dwarf mass M_*. The results are shown in Figure 23 for a stellar mass $M_* = 1M_\odot$ and rocky planet mass $m_{\rm p} = 1M_\oplus$. When the rocky planet is within the radius of the white dwarf, the tidal force per unit mass is of order 10^5 times greater than the rocky planet's surface gravity. Outside, the tidal disruption remains significant out to $r \sim 100R_*$. For a white dwarf of radius $R_* \sim 0.01R_\odot$, this corresponds to a sphere with radius $r \sim 1R_\odot$. Any rocky bodies entering this region will be tidally destroyed and can be accreted onto the central star. Rocky planets and asteroids can thus be easily captured and destroyed by white dwarfs.

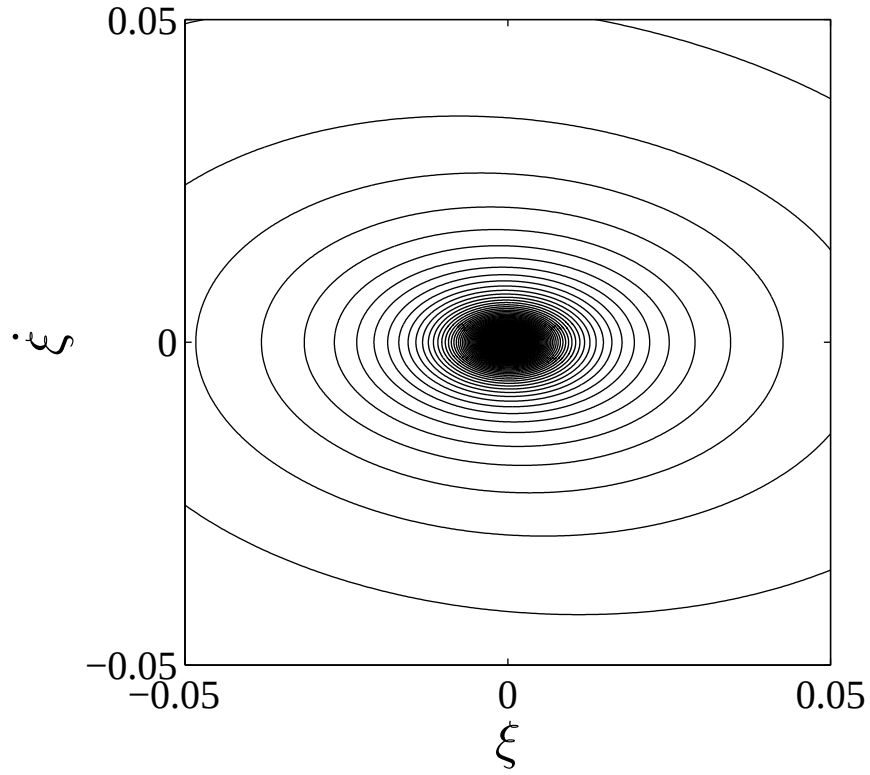

Fig. 21.— Motion of the test particle in the phase space $(\xi, \dot{\xi})$ for small radial coordinate ξ. The particle has impact parameter $x_0 = 0$ (i.e., the motion is purely radial), and oscillates continuously through the origin. As the particle approaches the origin (in phase space), the spacing between the orbits decreases, and eventually the individual orbits cannot be distinguished. Although this plot clearly indicates that the damping decreases with time, it is unclear whether the particle will come to rest in a finite amount of time, or continue to oscillate about the origin indefinitely.

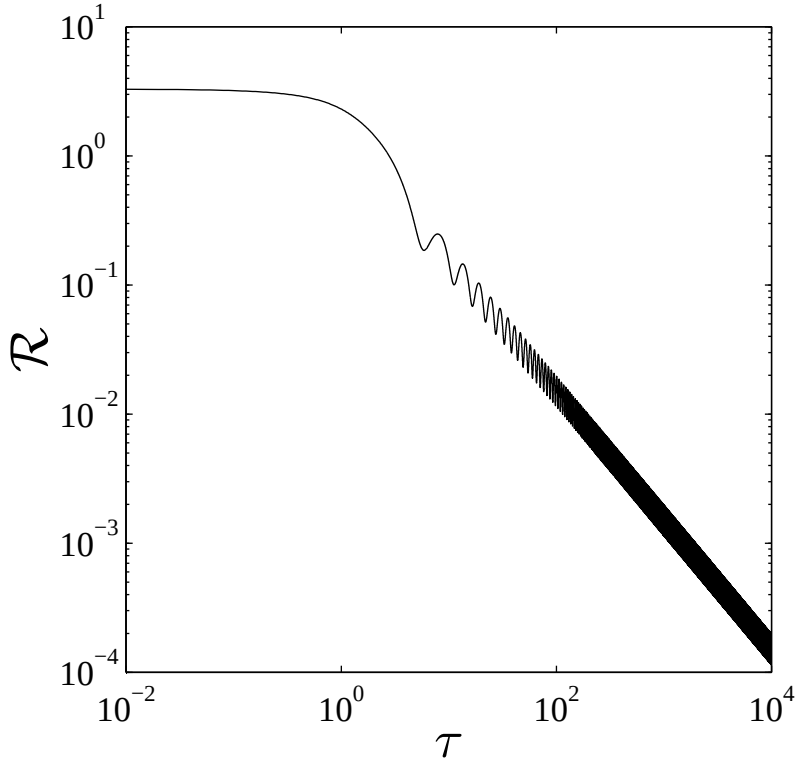

Fig. 22.— Graph of the energy-like function $\mathcal{R} = \left(\xi^2 + \dot{\xi}^2\right)^{1/2}$ as a function of time. After the initial transient behavior dies away, the slope of $\mathcal{R}$ (indicating the degree to which the particle's energy decreases) approaches a constant value for large time. In other words, as $\tau \to \infty$, the functional form for $\mathcal{R}(\tau)$ approaches a power-law (see equation [B1]). This suggests that the particle will oscillate indefinitely and approach the origin asymptotically.

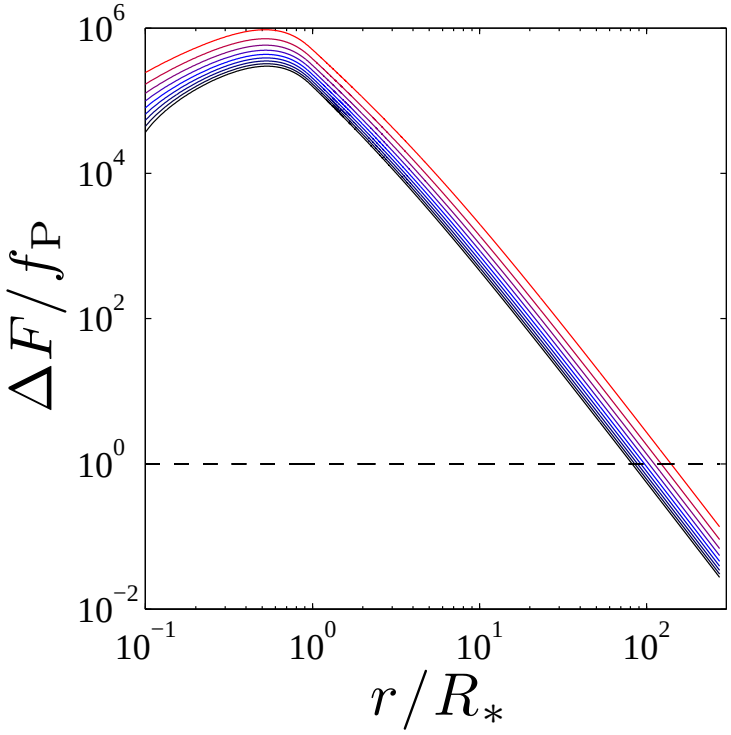

Fig. 23.— Tidal forces exerted on a rocky planet of mass $m_{\rm p} = 1 M_\oplus$ by a white dwarf of mass $M_* = 1 M_\odot$ as a function of radial distance. Each curve corresponds to a different mean density for the rocky planet, ranging from 2 (top red), to 10 (bottom black) g cm^{-3}. The rocky planet can avoid tidal destruction only when the curves are below the dashed line, where $\Delta F / f_{\rm p} < 1$. For distances $r \lesssim 100 R_* \approx 1 R_\odot$, the rocky planet experiences severe tidal disruption, and approaches a maximum within the radius of the white dwarf, where the ratio $\Delta F / f_{\rm p} \approx 10^6$. The sphere of destruction surrounding a white dwarf is large, and such stars can easily destroy planets and asteroids and thus accrete significant amounts of rocky material, given a plentiful supply of rocky bodies near this feeding zone.

REFERENCES

Abramowitz, M., & Stegun, I. A., 1970, Handbook of Mathematical Functions (New York: Dover)

Adams, F. C., & Bloch, A. M. 2009, ApJ, 701, 1381

Anic, A., Alibert, Y., & Benz, W. 2007, A&A, 466, 717

Arras, P., Socrates, A. 2010, ApJ, 714, 1

Artymowicz, P. 1993, ApJ, 419, 166

Baraffe, I., Chabrier, G., & Barman, T. 2010, Reports on Progress in Physics, 73, 016901

Batygin, K., & Stevenson, D. J. 2010, ApJ, 714, 238

Batygin, K., Stevenson, D. J., & Bodenheimer, P. H. 2011, ApJ, 738, 1

Benvenuto, O. G., Brunini, A. 2008, Icarus, 195, 882

Bodenheimer, P., Laughlin, G., & Lin, D.N.C. 2003, ApJ, 592, 555

Boley, A. C. 2009, ApJ, 695, 53

Borucki, W. J., Koch, D. G., Basri, G., et al. 2011, ApJ, 736, 19

Boss, A. P. 1997, Science, 276, 1836

Bramich, D. M., & Horne, K. 2006, MNRAS, 367, 1677

Burrows, A., et al. 1997, ApJ, 491, 856

Burrows, A., Hubeny, I., Budaj, J., & Hubbard, W. B. 2007, ApJ, 661, 502

Burrows, A. 2011, private communication

Chandrasekhar S, 1939 An Introduction to the Study of Stellar Structure (Chicago: University Chicago Press)

Crida, A., Sandor, Z., & Kley, W. 2008, A&A, 483, 325

Fortney, J. J., Saumon, D., Marley, M. S., Lodders, K., & Freedman, R. S. 2006, ApJ, 642, 495

Guillot, T., Showman, A. P. 2002, A&A, 385, 156

Gu, P., Bodenheimer, P. H., & Lin, D. N. C. 2004, ApJ, 608, 1076

Helled, R., Podolak, M., & Kovetz, A. 2006, Icarus, 185, 64

Helled, R., Schubert, G. 2009, ApJ, 697, 1256

Hubbard, W. B., Burrows, A. & Lunine, J. I. 2002, ARA&A, 40, 130

Ikoma, M., Guillot, T., Genda, H., Tanigawa, T., & Ida S. 2006, ApJ, 650, 1150

Jura, M., 2003, ApJ, 584, L91

Ketchum, J. A., Adams, F. C., & Bloch, A. M. 2011a, ApJ, 726, 53

Ketchum, J. A., Adams, F. C., & Bloch, A. M. 2011b, ApJ, 741, L2

Kley, W., Peitz, J., & Bryden, G. 2004, A&A, 414, 735

Laughlin, G., Crismani, M., & Adams, F. C. 2011, ApJ, 729, L7

Li, S. L., Agnor, C. B., & Lin, D. N. C. 2010, ApJ, 720, 1161

Mayor, M., & Queloz, D. 1995, Nature, 378, 355

Militzer, B., Hubbard, W. B., Vorberger, J., Tamblyn, I., & Bonev, S. A. 2008, ApJ, 688, L45

Papaloizou, J. C. B., Terquem, C. 2006, Reports on Progress in Physics, 69, 119

Perna, R., Menou, K., Rauscher, E. 2010, ApJ, 724, 313

Phillips, A. C. 1994, The Physics of Stars (Chichester: Wiley)

Pollack, J. B., Hubickyj, O., Bodenheimer, P., Lissauer, J. J., Podolak, M., & Greenzweig, Y. 1996, Icarus, 124, 62

Press, W. H., Teukolsky, S. A., Vetterling, W. T., & Flannery, B. P. 1992, Numerical Recipes in FORTRAN: The Art of Scientific Computing (Cambridge: Cambridge Univ. Press)

Prialnik, D. 2010, An Introduction to the Theory of Stellar Structure and Evolution (Cambridge: Cambridge Univ. Press)

Rauscher, E., Menou, K. 2012, ApJ, 745, 78

Sato, B. et al. 2005, ApJ, 633, 465

Saumon, D., Guillot, T. 2004, ApJ, 609, 1170

Sudarsky, D., Burrows, A., Pinto, P., ApJ, 538, 885

Valencia, D., Sasselov, D. D., & O'Connell, R. J. 2007, ApJ, 665, 1413

van Saders, J. L., & Gaudi, B. S. 2011, ApJ, 729, 63

Vennes, S., Kawka, A., Nemeth, P. 2010 MNRAS, 404, L40

Table 1. Polytrope properties as a function of dimensionless core radius ξ_c for polytropic index $n = 1$. The dimensionless radius ξ_0 and mass μ_0 have been calculated by numerically integrating the Lane-Emden equation (4). Central pressure ρ_c, core mass M_c and core radius R_c, collapse time t_0 and characteristic velocity R/t_0 have been calculated by assuming a total Jovian planet mass $M_P = 1M_J$ and radius $R_P = 1R_J$.

ξ_c	ξ_0	μ_0	ρ_c (g cm^{-3})	R_c ($R_\oplus$)	M_c ($M_\oplus$)	t_0 (s)	R/t_0 (km s^{-1})
0.000	3.142	3.142	4.328	0.000	0.000	525.054	42.437
0.100	3.142	3.158	4.307	0.371	0.033	526.334	42.329
0.200	3.144	3.209	4.247	0.742	0.263	530.010	42.005
0.300	3.150	3.298	4.156	1.111	0.864	535.766	41.476
0.400	3.161	3.426	4.043	1.476	1.971	543.237	40.764
0.500	3.178	3.595	3.915	1.836	3.670	552.036	39.901
0.600	3.201	3.805	3.780	2.187	5.990	561.795	38.923
0.700	3.231	4.058	3.644	2.528	8.919	572.187	37.865
0.800	3.267	4.354	3.511	2.857	12.409	582.932	36.758
0.900	3.309	4.695	3.384	3.173	16.387	593.811	35.627
1.000	3.356	5.080	3.263	3.476	20.774	604.648	34.494
1.100	3.409	5.511	3.151	3.765	25.487	615.319	33.375
1.200	3.466	5.989	3.047	4.040	30.446	625.732	32.280
1.300	3.526	6.516	2.951	4.301	35.580	635.824	31.219
1.400	3.591	7.093	2.863	4.548	40.825	645.559	30.195
1.500	3.659	7.721	2.782	4.783	46.128	654.911	29.213
1.600	3.729	8.402	2.707	5.005	51.445	663.875	28.273
1.700	3.803	9.137	2.638	5.216	56.740	672.447	27.376
1.800	3.878	9.929	2.575	5.415	61.983	680.635	26.521
1.900	3.955	10.779	2.517	5.604	67.152	688.449	25.707
2.000	4.034	11.688	2.464	5.784	72.230	695.901	24.933

Table 2. Same as Table 1, but polytropic index $n = 1.5$.

ξ_c	ξ_0	μ_0	ρ_c (g cm^{-3})	R_c ($R_\oplus$)	M_c ($M_\oplus$)	t_0 (s)	R/t_0 (km s^{-1})
0.000	3.654	2.714	7.922	0.000	0.000	388.079	49.368
0.100	3.650	2.725	7.863	0.320	0.039	389.530	49.239
0.200	3.640	2.762	7.694	0.641	0.306	393.778	48.841
0.300	3.627	2.830	7.434	0.965	1.007	400.603	48.171
0.400	3.616	2.932	7.109	1.291	2.304	409.666	47.254
0.500	3.608	3.070	6.746	1.617	4.298	420.552	46.129
0.600	3.606	3.246	6.368	1.941	7.023	432.830	44.846
0.700	3.611	3.463	5.995	2.261	10.456	446.092	43.453
0.800	3.624	3.719	5.640	2.576	14.531	459.948	41.999
0.900	3.644	4.018	5.308	2.882	19.152	474.099	40.520
1.000	3.671	4.359	5.004	3.178	24.215	488.284	39.049
1.100	3.706	4.744	4.728	3.463	29.615	502.336	37.605
1.200	3.746	5.174	4.479	3.737	35.253	516.105	36.205
1.300	3.793	5.650	4.255	3.999	41.042	529.490	34.859
1.400	3.844	6.174	4.055	4.249	46.911	542.432	33.572
1.500	3.900	6.747	3.875	4.487	52.797	554.898	32.348
1.600	3.960	7.371	3.713	4.714	58.654	566.850	31.186
1.700	4.023	8.047	3.568	4.929	64.442	578.289	30.086
1.800	4.090	8.778	3.436	5.134	70.133	589.220	29.045
1.900	4.160	9.563	3.318	5.329	75.705	599.661	28.062
2.000	4.232	10.407	3.210	5.514	81.143	609.625	27.133

Table 3. Same as Table 1, but polytropic index $n = 2$.

ξ_c	ξ_0	μ_0	ρ_c (g cm^{-3})	R_c ($R_\oplus$)	M_c ($M_\oplus$)	t_0 (s)	R/t_0 (km s^{-1})
0.000	4.353	2.411	15.079	0.000	0.000	281.285	57.171
0.100	4.343	2.418	14.927	0.269	0.044	282.715	57.017
0.200	4.314	2.445	14.481	0.541	0.345	287.038	56.524
0.300	4.274	2.496	13.786	0.819	1.142	294.184	55.674
0.400	4.227	2.578	12.917	1.104	2.621	303.916	54.486
0.500	4.180	2.693	11.957	1.395	4.900	315.883	53.012
0.600	4.138	2.844	10.979	1.692	8.017	329.645	51.322
0.700	4.103	3.033	10.040	1.990	11.938	344.725	49.491
0.800	4.078	3.261	9.169	2.289	16.575	360.719	47.585
0.900	4.064	3.529	8.384	2.584	21.807	377.221	45.662
1.000	4.061	3.838	7.689	2.873	27.503	393.900	43.766
1.100	4.067	4.190	7.079	3.155	33.535	410.531	41.923
1.200	4.083	4.585	6.546	3.429	39.786	426.913	40.156
1.300	4.108	5.024	6.082	3.692	46.156	442.897	38.474
1.400	4.140	5.510	5.678	3.945	52.565	458.401	36.882
1.500	4.179	6.044	5.324	4.187	58.946	473.373	35.383
1.600	4.224	6.626	5.015	4.419	65.249	487.746	33.973
1.700	4.275	7.260	4.743	4.640	71.436	501.537	32.650
1.800	4.330	7.945	4.503	4.850	77.481	514.738	31.410
1.900	4.389	8.685	4.290	5.051	83.363	527.336	30.246
2.000	4.451	9.481	4.101	5.242	89.071	539.379	29.155